UPPSALA
UNIVERSITET

Digital Comprehensive Summaries of Uppsala Dissertations from the Faculty of Science and Technology 1262

Computerized Cell and Tissue Analysis

AZADEH FAKHRZADEH

ACTA
UNIVERSITATIS
UPSALIENSIS
UPPSALA
2015

ISSN 1651-6214
ISBN 978-91-554-9269-4
urn:nbn:se:uu:diva-252425

Dissertation presented at Uppsala University to be publicly examined in 2446, ITC, Polacksbacken, Lägerhyddsvägen 2, Uppsala, Friday, 12 June 2015 at 09:15 for the degree of Doctor of Philosophy. The examination will be conducted in English. Faculty examiner: Associate Professor Nasir Rajpoot (University of Warwick).

Abstract

Fakhrzadeh, A. 2015. Computerized Cell and Tissue Analysis. *Digital Comprehensive Summaries of Uppsala Dissertations from the Faculty of Science and Technology* 1262. 63 pp. Uppsala: Acta Universitatis Upsaliensis. ISBN 978-91-554-9269-4.

The latest advances in digital cameras combined with powerful computer software enable us to store high-quality microscopy images of specimen. Studying hundreds of images manually is very time consuming and has the problem of human subjectivity and inconsistency. Quantitative image analysis is an emerging field and has found its way into analysis of microscopy images for clinical and research purposes. When developing a pipeline, it is important that its components are simple enough to be generalized and have predictive value. This thesis addresses the automation of quantitative analysis of tissue in two different fields: pathology and plant biology.

Testicular tissue is a complex structure consisting of seminiferous tubules. The epithelial layer of a seminiferous tubule contains cells that differentiate from primitive germ cells to spermatozoa in a number of steps. These steps are combined in 12 stages in the cycle of the seminiferous epithelium in the mink. The society of toxicological pathology recommends classifying the testicular epithelial into different stages when assessing tissue damage to determine if the dynamics in the spermatogenic cycle have been disturbed. This thesis presents two automated methods for fast and robust segmentation of tubules, and an automated method of staging them. For better accuracy and statistical analysis, we proposed to pool stages into 5 groups. This pooling is suggested based on the morphology of tubules. In the 5 stage case, the overall number of correctly classified tubules is 79.6%.

Contextual information on the localization of fluorescence in microscopy images of plant specimen help us to better understand differentiation and maturation of stem cells into tissues. We propose a pipeline for automated segmentation and classification of the cells in a whole cross-section of Arabidopsis hypocotyl, stem, or root. As proof-of-concept that the classification provides a meaningful basis to group cells for fluorescence characterization, we probed tissues with an antibody specific to xylem vessels in the secondary cell wall. Fluorescence intensity in different classes of cells is measured by the pipeline. The measurement results clearly show that the xylem vessels are the dominant cell type that exhibit a fluorescence signal.

Keywords: Image processing, Cell, Tissue, Segmentation, Classification, Histology

Azadeh Fakhrzadeh, Department of Information Technology, Division of Visual Information and Interaction, Box 337, Uppsala University, SE-751 05 Uppsala, Sweden.

ISSN 1651-6214
ISBN 978-91-554-9269-4
urn:nbn:se:uu:diva-252425 (http://urn.kb.se/resolve?urn=urn:nbn:se:uu:diva-252425)

To my dear family

List of papers

This thesis is based on the following papers, which are referred to in the text by their Roman numerals.

I Azadeh Fakhrzadeh, Ellinor Spörndly-Nees, Lena Holm and Cris L. Luengo Hendriks, *Analyzing Tubular Tissue in Histopathological Thin Sections.* In proceedings of 2012 International Conference on Digital Image Computing Techniques and Applications (DICTA2012), pp. 1-6, Fremantle, Australia, December 3-5, 2012.

II Azadeh Fakhrzadeh, Ellinor Spörndly-Nees, Abdolrahim Kadkhodamohammadi, Lena Holm and Cris L. Luengo Hendriks, *Epithelial Cell Segmentation in Histological Images of Testicular Tissue Using Graph-Cut.* In proceedings of 17th International Conference on Image Analysis and Processing (ICIAP2013), pp. 201-208, Naples, Italy, September 9-13, 2013.

III Azadeh Fakhrzadeh, Ellinor Spörndly-Nees, Elisabeth Ekstedt, Lena Holm and Cris L. Luengo Hendriks, *Computerized Study of Developmental Stages in Mink Testicular Tissue.*

IV Hardy Hall, Azadeh Fakhrzadeh, Cris L. Lunego Hendriks, Urs Fischer, *Precision Automation of Cell type Classification and Sub-cellular Fluorescence Quantification from Laser Scanning Confocal Images.*

V Ellinor Spörndly-Nees, Elisabeth Ekstedt, Ulf Magnusson, Azadeh Fakhrzadeh, Cris L. Luengo Hendriks, Lena Holm, *Effect of Pre-Fixation Delay and Freezing on Mink Testicular Endpoints for Environmental Research*, PLoS ONE 10(5): e0125139. doi: 10.1371/journal.pone.0125139.

I developed all image analysis and pattern recognition tools described in the five papers, wrote papers I-II, and contributed to the writing of papers III-V. Reprints were made with the permission from the publishers.

Related work

In addition to the papers included in this thesis, I have also written following publications:

1. Azadeh Fakhrzadeh, Ellinor Spörndly-Nees, Lena Holm and Cris L. Luengo Hendriks, *Automated Measurement of Epithelial Height of Testicular Tissue*, In Proceedings of Swedish Symposium on Image Analysis (SSBA 2012), Stockholm, Sweden, March 7-8, 2012.

2. Azadeh Fakhrzadeh, Ellinor Spörndly-Nees, Lena Holm and Cris L. Luengo Hendriks, *Epithelial Cell Layer Segmentation Using Graph-Cut and Its Application in Testicular Tissue*, In Proceedings of Medical Image Understanding and Analysis (MIUA 2013), Birmingham, United Kingdom, July 17-19, 2013.

Contents

1. Introduction

1.1 Motivation

Digitalization of biological data has enabled us to use computer systems to assist doctors and researchers in interpretation and analyzing the data. Recent advances in image acquisition and analysis, together with improvements in microprocessor performance, have brought automated image processing methods within reach. In the absence of automated methods, analysis of the digital images is qualitative and labor-intensive, and has the problem of human subjectivity and inconsistency. With emerging imaging tools, quantitative image analysis can assist technicians and doctors to make more accurate diagnosis. Challenges in computer assisted analysis are the accuracy and speed for proving a useful outcome and at the same time handling enormous data involved in digital samples [2]. Another challenge is to make the methods usable for the biologists [2]. There is always a trade-off between the simplicity of use and flexibility for diverse and complex applications. In this thesis we addressed two issues in microscopy image analysis. One of them relates to analyzing histopathological images of testicular tissue. The other one deals with a quantification of gene expression in fluorescent images of plant cells.

Testicular tissue is a complex structure consisting of seminiferous tubules. The epithelium layer of seminiferous tubules contains cells which differentiate from primitive germ cells to spermatozoa in a number of steps. These steps are combined in twelve stages in the cycle of the seminiferous epithelium in the mink. Segmenting the epithelium of tubules and classifying them to known stages can assist pathologist in interpretation of the sectioned tissue.

Contextual information on the localization of fluorescence in microscopy images of plant specimen helps us in better understanding of differentiation and maturation of stem cells into tissues. Changes in morphology and wall composition are indicative for the degree of differentiation and cell type. Segmenting cells and classifying them in different cell types provide the ability to perform statistical analysis and quantification of fluorescence on a specific cell type.

For both types data sets I) I suggest automated segmentation method for segmenting regions of interest (ROIs), II) propose classification methods to classify ROIs into categories defined by an expert, III) perform statistical analysis of ROIs.

1.2 Outline of Thesis

The outline of this thesis is as follows: Chapter two is an overview of segmentation methods. Chapter three is an overview of classification and feature extraction methods. In both these chapters the main focus is on methods that are used later in contribution chapters. Chapter four and five are detailed descriptions of two developed pipelines. Chapter four starts with an overview of testicular tissue and addresses a classification problem for stained testicular tissue. Then a pipeline is suggested to automate the analysis. Chapter five starts with an overview of fluorescent images of cross section of plant. In this chapter a detailed pipeline for measuring florescence with sub-cellular resolution is proposed and discussed. In chapter six I make concluding remarks and give some suggestions for future work.

2. Segmentation

Image segmentation is the process of partitioning an image into disjoint subdivisions. Every subdivision usually has similar properties such as similar intensity value or texture. Segmentation is one the most important steps in an image analysis pipeline. All further analysis such as feature extraction and classification are dependent on the result of segmentation. Some of the segmentation methods, like thresholding, are largely based on ad-hoc ideas. Although these methods are not robust, they are widely used because of their simplicity and speed.

In energy based segmentation methods, segmentation is the result of minimizing an energy function. The energy function can be defined in the continuous domain or the discrete domain. Snakes [24, 48] and Level set segmentation methods [19, 20, 58, 60] are examples of continuous domain methods and graph based segmentation methods [13, 39, 79] are examples of discrete domain methods.

Active contour or Snakes is an evolving interface whose motion is guided by internal and external forces. The external force is defined based on regional properties of the image. In Snakes, we define an initial curve for every object, the curve grows until it reaches the boundaries. This method has some limitations, for example the initial curves cannot split or merge, and they can only grow or shrink. This can be problematic if topology of the object is changed. The level set method, which is also an evolving interface, can handle topology changes such as self-intersection better than Snakes.

Graph based segmentation treats an image as a graph where neighboring pixels are connected by edges weighted based on intensity similarity between pixels. Segmentation is performed by minimizing the sum of edge weights for background and foreground.

Watershed segmentation is a morphology based image segmentation. In Watershed segmentation [8, 9, 85] a grey level image is considered as a landscape. Low intensity regions are valleys in the landscape and high intensity are hills. The landscape is immersed in water and water is flooded from local minima. A dam is placed where the water from two different catchment basins meets. Watershed segmentation can be implemented as an energy based segmentation using a graph [28].

Another segmentation method based on graphs is Livewire [5]. Livewire is an interactive segmentation method. This technique requires the user to place a point along the boundary of the desired object, the algorithm

calculates the cost of the optimal path between this seed point and all other pixels in the image. With the help of the algorithm the user can select the next point on the boundary whose path cost to the seed point is minimum. These segmentation methods will be described in more detail in this chapter.

2.1 Level Set Segmentation

The Level set was first proposed by Osher and Sethian [70] as a numerical method for computing the motion of an interface. Caselles et al. [19] and Malladi et al. [60] used Level set in the context of Snakes models for image segmentation. In the Level set segmentation, the evolving curves are actually the zero iso-contours of a Level set function $\phi(x, y, t) : \Omega \longrightarrow R$, where Ω is the domain of an image. The Level set function changes with time and evolving contours are computed indirectly as its zero contours where $\phi(x, y, t) = 0$. The equation for the motion of the interface is

$$\frac{\partial \phi}{\partial t} + F|\nabla \phi| = 0, \tag{2.1}$$

where F is a function that models the desired velocity on the interface and ∇ is the gradient operator. The interior and exterior of ϕ in the region Ω are respectively defined as $\{(x, y) \in \Omega | \phi(x, y, t) < 0\}$ and $\{(x, y) \in \Omega | \phi(x, y, t) > 0\}$. The most difficult task is to establish a Level set function that can make a meaningful segmentation of a desired object in the image. Li and Xu [58] suggested an energy function for the Level set which includes both the edge and region information. If image I belongs to domain Ω, the edge indicator can be defined as:

$$g = \frac{1}{1 + |\nabla G_\sigma * I|^2} , \tag{2.2}$$

where G_σ is a zero-mean Gaussian distribution with standard deviation of σ and operator $*$ is convolution. The function g usually has smaller values at object boundaries than at other locations in the image. For a Level set function ϕ, Li and Xu [58] suggested following energy function:

$$\begin{aligned} E(\phi) &= \mu \int_\Omega p(|\nabla \phi|) dx + \lambda \int_\Omega g\delta(\phi)|\nabla \phi| dx \\ &+ \alpha \int_\Omega gH(-\phi) dx . \end{aligned} \tag{2.3}$$

The first part of this equation is the Level set regularization term, where p is the energy density function and μ, λ and α are energy coefficients,

and δ and H are the Dirac delta and the Heaviside functions, respectively. The coefficient α can have a negative or a positive value depending on whether the initialized contour is inside or outside of the object. This energy function is minimized when the contours reach the boundary of the object. With the Dirac delta function, the second part of energy function is the integral along the zero level contour of ϕ. The last term is proportional to the area of the interior of ϕ and is used to speed up the motion when the zero level contour is placed far away from the object boundary.

2.2 Graph Cut Segmentation

Wu and Leahy [90] and Zahn [91] are among the first people who applied graph theory in image processing applications. This got a great deal of attention in segmentation after Shi and Malik [79] introduced the normalized cuts algorithm. A graph $g = \{\nu, \varepsilon, \omega\}$ is defined as a set of nodes, or vertices, $\nu = \{v_i\}$ and a set of edges $\varepsilon = \{e_{ij}\}$ with weights $\omega = \{w_{ij}\}$, e_{ij} is the edge between nodes v_i and v_j and w_{ij} is its corresponding weight. A directed graph is a graph whose edges have a direction associated with them. An $s-t$ graph is a directed weighted graph with two specific nodes called the source s and the sink t.

An $s-t$ cut is a subset of edges $C \subset \varepsilon$ such that the terminals s and t become completely separated on the induced graph $g = \{\nu, \varepsilon - C\}$. The cost for a cut $|C|$ is the sum of the costs of all the edges it contains, see figure 2.1.

The minimum cut problem is to minimize the cost $|C|$, which is to find an $s-t$ cut with minimum cost. Based on combinational optimization, a globally minimal $s-t$ cut can be computed efficiently in low order polynomial time.

Graph-cut segmentation methods became popular after Boykov et al. [15] published a new and often fast approach for image segmentation [13, 14, 15]. In binary segmentation every pixel $p \in P$ is assigned a label $f_p \in \{0, 1\}$; if p is in the object then $f_p = 1$ and if p is in the background then $f_p = 0$. Segmentation can be accomplished by defining a proper energy function whose optimization gives the best labelling. The general form of the energy function is defined as follows:

$$E(f) = \lambda \sum_{p \in P} D_p(f_p) + \sum_{\{p,q\} \in N} V_{pq}(f_p, f_q) \tag{2.4}$$

where N is the set of neighborhood pixels, D_p is called the data term and is the cost of assigning f_p to the pixel p, V_{pq} is called the regularization or smoothness term and is the cost of assigning f_p to pixel p and f_q to pixel q, and λ is a coefficient for balancing between D_p and V_{pq}.

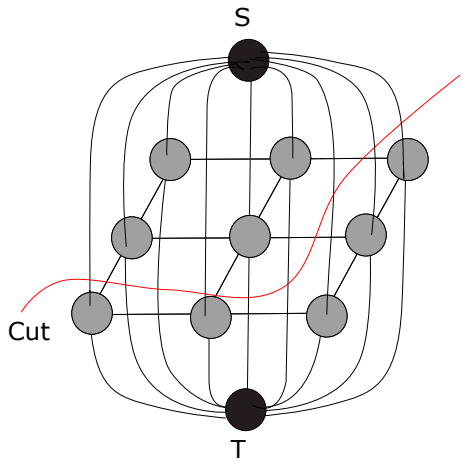

Figure 2.1. *Graph cut segmentation, where Source (S) and sink (T) become separated by a cut (red dashed line).*

The regularization term penalizes the number of label transitions, and in energy minimization the penalty is smaller when two neighbor pixels are labeled the same. One of the main challenges in this procedure is computational time in minimizing the energy function. Boykov et al. [15] suggested limited types of smoothness assumption and showed that with a proper choice of edge weight one can minimize the energy function in equation 2.4 in reasonable time. Binary Graph cut segmentation of grey level images can be extended to multi-label segmentation with a one versus the rest strategy, or multi-cut.

2.3 Watershed Segmentation

In the Watershed segmentation a grey level image is regarded as a landscape, see figure 2.2. There are different ways of implementing Watershed. Beucher and Meyer [9] used a priority queue: first we find the local minima and then we assign different label to every minimum (seed). Neighboring pixels of seeds are prioritized based on their similarity to the seed intensity. The pixel with the highest priority is extracted from the queue, and is assigned the same label as its neighbors. If its neighbors do not share the same label, it does not get any label. Non-labeled pixels will be the Watershed dam. The same concept can be implemented using a graph [28]. Pixels are nodes in the graph which are connected with weighted edges. Weights represent the similarity between pixels and seed points. In this case, the edges adjacent to the seeds are added in a priority queue, where the priority is the weight of the edges.

In the Watershed method local minima are very important. Local minima can be computed directly from the image or its gradient or can be determined by the user. Every region of interest should have one local minimum, otherwise the Watershed dam, or object borders, are placed in a wrong position and the image is oversegmented. There are several approaches to solve this oversegmentation problem. For example, we can pre-process the image to filter out non-significant minima [75]. Alternatively, the image can be post-processed after the segmentation, oversegmented regions are merged based on some predefined condition such as similarity in average intensity offset [86]. The original Watershed segmentation method does not include any smoothness prior, and Watershed dams can be noisy. Nguyen et al.[67] represented Watershed segmentation method as an energy minimization problem and imposed smoothness as a term in the energy function.

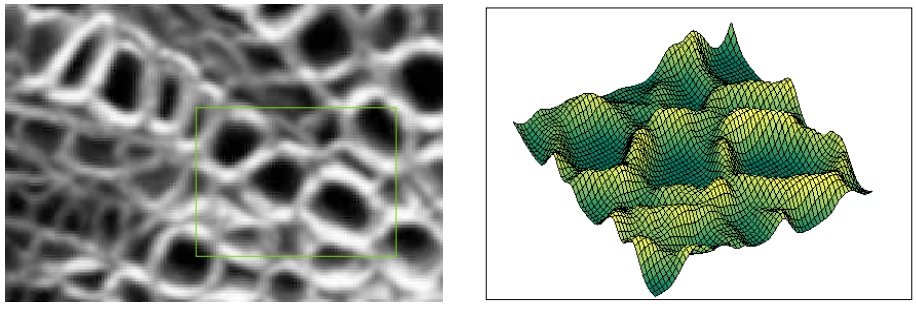

Figure 2.2. *On left is original image and a landscape representation of a part of it, marked with green box is shown in right.*

2.4 Livewire Segmentation

Livewire [5, 35] is a graph based segmentation method. In the graph representation, the weights assigned to edges are function of the boundary strength between two pixels in the image. In the Livewire algorithm the user need to specify a seed point. For delineating the object boundary the seed point should be paced on the object boundary. The shortest path between the seed point and all other pixels is calculated using Dijkstra's algorithm [33]. The user then can, by moving the mouse over the image, instantly see the optimal boundary between that seed point and the current mouse position. By clicking, the portion between the seed and click point gets fixed, and the newly selected pixel becomes the new seed point. The whole process is repeated. In this manner, the user can, interactively and with only a few clicks, very precisely delineate the whole object boundary.

3. Classification

3.1 Feature Selection and Extraction

In an image analysis pipeline, the next step after segmentation is classification of regions of interest or objects to different groups. To do so we need to map every object in an image to a vector that can describe the property of that object. This vector is called feature vector. To make classification easier, it is better that feature vectors of different objects have discriminatory information and as little overlap as possible. Irrelevant and redundant features can, in certain cases, make the classification worse. Reducing the number of features used as input to a classifier is referred to as dimensionality reduction, because the n features are seen as spanning an n-dimensional space. There are two ways of reducing the dimensionality: feature selection and feature extraction. The former selects the best subset of features, whereas the latter combines features to produce a reduced set. We lose interpretability of the classifier, with feature extraction, even if it potentially improves classification. Feature selection methods are a better choice if we want to interpret the effects of each original feature on the classification results [88].

In feature selection methods, we need a search algorithm that determines the best subset of features to use. The naive search algorithm considers all subsets, and hence is a very expensive approach: selecting k features out of n requires evaluating $\binom{n}{k} = \frac{n!}{(n-k)!k!}$ combinations. If we also want to find out how many features to keep, the number of combinations to evaluate grows rapidly. Other approaches have been suggested that are suboptimal but computationally feasible. Sequential Forward Selection (SFS) and Sequential Backward Section (SBS) are examples of such approaches. For both SFS and SBS we need to define a proper criterion function. SFS is a bottom-up search that adds one feature at the time until the desired number of features that maximizes the criterion function is obtained. On the other hand, SBS is a top down search algorithm which starts with all features, and then the worst features are removed one at the time.

In a feature extraction method, we replace original features with a smaller set of underlying variables. Leaner feature extraction methods such as Principal Component Analysis (PCA) [72] and Linear Discriminant Analysis (LDA) [36] seek for a linear combination of features that

best explain the data. PCA does not consider grouping or class of samples and is an unsupervised feature extraction method. The objective in PCA is to find an orthogonal transformation such that derived variables are uncorrelated. Principal components are obtained by eigendecomposition of the covariance matrix of features. The first principal component is aligned with the direction of largest variation of data.

LDA is a supervised feature extraction method. In LDA, the objective is to maximize between-class separability and to minimize within-class variation. The axes of the transformed system are ordered in terms of discrimination importance. LDA can be used for visualization of high dimensional data as well. In these cases we only consider the first two or three dimensions of the derived data.

3.2 Classification Methods

3.2.1 Support Vector Machine

Support vector machine (SVM) classifier [25] has a strong mathematical foundation. In binary classification, SVM constructs a hyperplane which has the largest distance to its nearest training points of any class. In other words, SVM maximizes the margin between two classes and this margin is the distance between two canonical hyperplanes that have no points between them. The separating hyperplane is half way in the middle of these two canonical hyperplanes. In linear SVM, the separating hyperplane is $\mathbf{w}^T\mathbf{x} + b = 0$, and two canonical hyperplanes are $\mathbf{w}^T\mathbf{x} + b = 1$ and $\mathbf{w}^T\mathbf{x} + b = -1$, where $\mathbf{w}$ denotes the normal vector to the hyperplanes. The distance for a point x_0 to the separating hyperplane is

$$d = \frac{|\mathbf{w}^T\mathbf{x_0} + b|}{\|\mathbf{w}\|} \tag{3.1}$$

The margin between two canonical hyperplines is $\frac{2}{\|\mathbf{w}\|}$, and maximizing this margin is equivalent to minimizing $\|\mathbf{w}\|$. The constraint for minimizing $\|\mathbf{w}\|$ is that there is no object between two hyperplanes. This is a constrained optimization problem that can be solved by the Lagrangian multiplier method. For the cases that data is not linearly separable, soft support vector machine introduces a slack variable ξ_i, which allows for a softer margin:

$$\begin{aligned} \underset{\mathbf{w},\xi,b}{\text{minimize}} \quad & \frac{1}{2}\|\mathbf{w}\|^2 + C\sum_{i=1}^{n}\xi_i, \\ \text{subject to} \quad & y_i(\mathbf{w}^T\mathbf{x_i} + b) \geq 1 - \xi_i, \;\; \xi_i \geq 0. \end{aligned} \tag{3.2}$$

The slack variables, ξ_is, measures the degree of misclassification, and the coefficient C is used to control the trade-off between the maximum margin and the misclassification error.

Non-linear SVM maps data into a higher dimensional space in the hope to gain less overlap between classes, so that linear SVM can be used. A linear boundary in the higher dimensional space corresponds to a complex decision boundary in the original feature space. Instead of computing the mapping, we can replace the original inner product of the objects, which is involved when solving the optimization problem, with the inner product of a kernel function [12]. Popular kernel functions are radial basis function, Gaussian, and low degree polynomial. SVM is frequently used in histopathology applications [26, 34, 87]. We also used it in papers III and chapter 5.

3.2.2 Decision Tree

A decision tree classifier [17] is a classification in the form of a tree: it consists of a root node, some internal nodes called decision nodes, and terminal nodes called leaf nodes. Every decision node establishes a threshold on a single feature, and has two branches; every leaf node contains a classification label. An object to be classified will traverse the tree, starting at the root node. At each decision node, one specific feature of the object is compared to the threshold, the result determines which of the two branches the object will follow. When a leaf node is reached, the object has been classified.

During training, a decision node is created that separates the training set into two groups, such that the entropy in each group is minimized. For each of these two groups, again a decision node is created in the same manner. This procedure is repeated recursively until a group contains only elements from a single class (the least entropy possible); a leaf node is created with the label for that class.

3.2.3 Random Forest

A Random Forest [16] is an ensemble classifier, combining many decision trees. It outputs the classification label most often returned by these trees (majority vote). To maximize the variation between trees, a different subset of the data is used to train each tree. These subsets are obtained by sampling the original data with replacement (bootstrap samples). The samples left out are called out-of-bag (OOB) data, and are used as test data to estimate the classification error of that tree. Feature importance is estimated as follows: feature m in the OOB data is randomly permuted. For every tree, the resulting classification error is

subtracted from the classification error of the untouched OOB data. The average of these values over all trees in the forest, normalized by their standard deviation, gives the importance score of feature m. Random Forest has been used for pathology applications [6, 31, 68] and we used it in IV and chapter 4.

3.2.4 RUSBoost

RUSBoost [77] is designed for imbalanced data sets, where RUS stands for random under sampling. It under-samples the majority class and uses the AdaBoost [38] method for training. AdaBoost is an ensemble classifier and consists of subsequent week learners. In AdaBoost, every observation has a weight. In the beginning the weights are uniform, for every learner weights get updated based on the result of previous learners. The objects misclassified by previous learners, get higher weights. The final result is the weighted sum of all week learner outputs. We used this method in chapter 4.

3.3 Evaluation

3.3.1 Confusion Matrix

When the data is unbalanced, overall accuracy of the classifier is misleading and biased toward the majority class. A confusion matrix can give the whole picture of the classification performance. In confusion matrix, each row represents instances in an actual class and each column represents instances in a predicted class. Samples on diagonal are samples which are correctly classified and other samples are misclassified samples.

3.3.2 Cross-validation

Cross-validation gives an unbiased estimate of a model performance. In cross-validation, the data set is randomly partitioned into two sets. The model parameters are estimated using one set and its performance is evaluated on the second set. In K-fold cross-validation, data is randomly divided into K equal size subsamples. One subsample is considered as the testing set and remaining $K-1$ samples as training set. The classifier is trained on $K-1$ subsamples, and the Kth subsamples is used to assess the classifier. The training is repeated K times, such that each of the subsamples is used once for assessment. The results from K folds are averaged.

3.4 Texture Features

3.4.1 Gabor Filters

A Gabor filter can be seen as a Gaussian kernel function modulated by a sinusoidal plane wave:

$$G(x, y, F, \theta, \sigma) = \frac{1}{\sqrt{2\pi}\sigma} \exp[\frac{-(x^2 + y^2)}{2\sigma^2}] \exp[i2\pi F(x\cos\theta + y\sin\theta)] \tag{3.3}$$

where σ is the standard deviation of Gaussian envelope (or scale), θ is the angle between direction of the wave and x-axis (or orientation) and F is the frequency of wave. Gabor filter bank is a set of Gabor filters with different scales, orientations and frequencies. Gabor filter bank has been used widely for calculating texture descriptor [4, 37, 45, 81, 89]. Bianconi and Fernndez [10] studied the effect of different parameters on texture discrimination and concluded that F and σ have the highest impact. They proposed the highest frequency F_M for every scale as:

$$F_M = \frac{\sigma}{2(\sigma + \sqrt{\log(2)}/\pi)} \tag{3.4}$$

If we want to have Gaussian filters with 3 different frequencies, the frequency set suggested by [10] is $\{F_1 = F_M, F_2 = \sqrt{2}F_1, F_3 = \sqrt{2}F_2\}$. One way of using Gabor filter bank as feature descriptor, is to apply every filter on an object and then use mean and standard deviation of the magnitude of the filters responses as the feature values. This method has been used in chapter 4.

3.4.2 Local Ternary Pattern

Local ternary pattern [82] is one of the variations of local binary pattern (LBP) [69]. LBP uses a local threshold to binarize the local neighborhood. The neighborhood is then summarized by concatenating binary pixel values into a single number. The distribution of local numbers are considered as feature vector. Ojala et al. [69] found that a small subset of binary codes that at most have two transitions between zero and one, corresponds to local structures such as edges, corners and spots. These subset of binary codes have the most discriminatory information of an object and are used as feature descriptors. Different LBPs based on choice of thereshold and the binarization method have been suggested. LTP for pixel c with intensity value g_c is defined as:

$$LTP_{N,R}(g_c, g_p, s, t) = \sum_{p=0}^{N-1} s(g_p, g_c, t)2^p, \tag{3.5}$$

where

$$s(g_p, g_c, t) = \begin{cases} 1, & g_p >= g_c + t, \\ 0, & g_c - t =< g_p < g_c + t, \\ -1, & \text{otherwise} \end{cases} \tag{3.6}$$

where N is number of points (p) at the distance of R of point c, g_p is intensity value of point p and t is a threshold. LBP is used in medical and histopatologycal application [63, 83, 78], we also used a rotation invariant LTP in paper III.

3.4.3 Rotation Invariant Texture Features

Many of texture descriptors are dependent on rotation. Some approaches have been suggested to make them rotation invariant. One straightforward method is to compute the average features corresponding to different orientations [42]. Another method circularly shifts features according to the dominant direction [4]. Another approach is based on a common property of the Fourier transform [81]: we know that translation in time corresponds to shift in phase in the Fourier transform. By considering only the magnitude of the Fourier transform of features, the shift is disregarded. The magnitude of the spectrum is symmetric so half of it can be discarded. This rotation invariant method has been used in paper III.

4. Automated Analysis of Histology Images of Testicular Tissue

4.1 Background

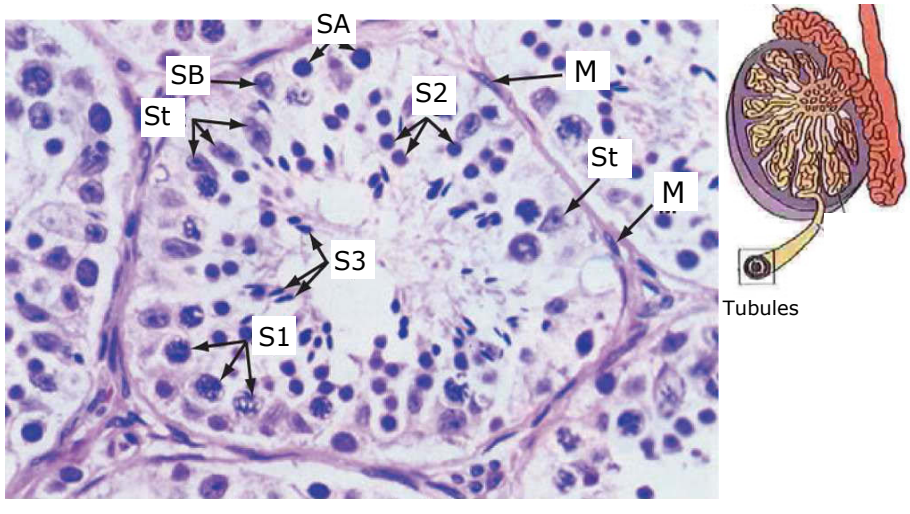

Figure 4.1. *On right is testis on left is histology image of a cross section of a seminiferous tubule. M: myoid cell just outside the basal lamina; S1: primary spermatocyte; S2: spermatid; S3: mature spermatid or spermatozoon; SB and SA: spermatogonia; St: Sertoli cell, figures from [51] and [61]*

The male reproductive system consists of penis, accessory glands, genital ducts and testis. Spermatoza are produced in the testis at a rate of 2×10^8 per day in a human male adult. Each testicle has 250-1000 seminiferous tubules, where each tubule measures about 150-250 μm. in diameter and 30-70 cm in length [66]. A seminiferous tubule is enclosed with a complex epithelium. The seminiferous epithelium has two types of cells: non-dividing sertoli cells (St in figure 4.1) and proliferative germ cells (S1, S2, S3, SA, SB in figure 4.1). The primitive germ cells (SA, SB) are small round cells which go through different stages of development to become spermatoza (sperm cells). Different stages

of development are recognized by the shape of the cell nuclei and their staining properties.

There are twelve different stages in the cycle of the seminiferous epithelium in mink, defined in detail by Pelletier [73], figure 4.2. The Society of Toxicological Pathology recommends classifying the testicular epithelium into different stages when assessing tissue damage to determine if the dynamics in the spermatogenic cycle has been disturbed [54]. If a toxicant affects the testis it might lead to a new combination of the cells in a certain stage. For example a particular cell type can be missing or an inappropriate cell type can be present in a certain stage due to exposure to a cytotoxic agent [30]. These changes may be the only morphological sign of toxic damage and it can only be detected by staging [52].

The quantitative analysis of digital pathology is important not only from a diagnostic perspective, but also in order to understand the underlying reasons for a specific diagnosis being rendered [41]. In this study we use image analysis techniques on microscopy images of testicular tissue from mink. Mink is a semi-aquatic top predator that has been suggested as a suitable sentinel species in environmental monitoring of endocrine disruptive chemicals [7, 74]. The aim of this study is to design a computerized method to determine the stages in histology images of mink testicle tissue. Our ultimate goal is to provide an objective tool that can be used by all pathologists, and which is adjustable to function for the analysis of tissue also from other species.

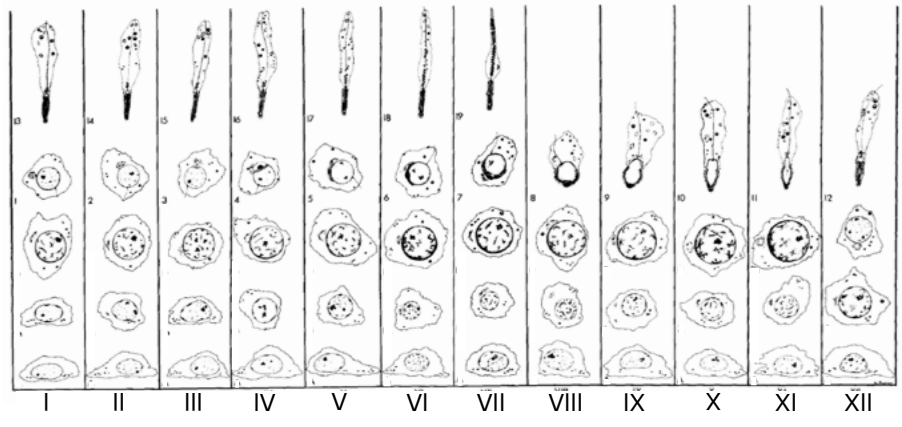

Figure 4.2. *The characteristic cellular composition of the 12 stages, figure form [73]*

4.2 Animals and Dissection

Four healthy, sexually mature minks were collected at the annual culling on a mink farm. No ethical approval was required due to the use of routinely culled mink from a fur farm. The commercial fur farm approved the use of the mink for the study. Transverse tissue slices from testis were fixed and embedded. The samples were cut in 5 micrometer sections and stained with Gata-4 antibody (brown) and and haematoxylin counterstain (blue). Digital images of the sections were taken with a Nikon Microphot-FXA microscope using the 20x objective lens. Size of images in pixel is 1200 by 1600 and pixel size is 0.4 μm. Images are RGB and for this analysis we only used channel R.

4.3 Algorithm

4.3.1 Segmentation

The first step in the algorithm is segmentation. One approach is to segment all the cells and classify them into different groups (S1-S3, SA-SC). Based on the type of the cells represented in each tubule, a stage is assigned to that tubule. There are thousands of cells in every tubule and every image in average contains around five tubules. These cells have arbitrary shapes and color content. This makes an automated segmentation and also classification of cells very challenging. Another direction is to segment each tubule and treat its area as a texture.

We have suggested two automated segmentation methods for two different stainings. For Periodic Acid Schiff (PAS) stained thin sections, we first delineate the border of lumen using the Level set segmentation method. The borders of tubules are then segmented using a thresholding method followed by an approach based on geodesic distance to correct undersegmentation (paper I).

For Gata-4 staining, the cell nuclei are first detected using the Fast Radial Symmetry filter [59]. A graph is constructed on top of the epithelium cells. Graph cut segmentation method is used to cut the links between cells of different tubules (paper II).

In papers III and V, we used a semi-automated Livewire segmentation method. The user adds a seed point on the boundary of a tubule, and the algorithm calculates the cost of the optimal boundary between this seed point and all other pixels in the image. By moving the mouse over the image, the user can then instantly see the optimal boundary between that seed point and the mouse position and delineate the tubules boundary. The semi-automated method is controlled by the user, and has fewer errors. This is the segmentation method we used before classification.

4.3.2 Feature Description

The next step after segmentation is to find features for every object of interest. Pathologists examine tubules locally and depending on cell types they contain assign a stage to them. One approach is to partition every tubule to patches or superpixels and for every patch find a feature vector. Patches are clustered into different categories and the histogram of different patch clusters within a tubule is considered as its feature vector. Superpixels have been used for glandular structures segmentation in colon histology images [80]. Exploitation of superpixels made the algorithm complicated without rendering a satisfactory results. We consequently decided to directly find a feature vector for every tubule.

Texture descriptors capture spatial relationship between pixels. Tubules with different cell types also are different in texture. We exploited two texture descriptors: Gabor filters [37] and Local Ternary Pattern (LTP)[82].

For this application, parameters of Gabor filter are four scales $\sigma = \{1, 3, 5, 7\}$, seven orientations uniformly distributed over π radian and four frequencies. The first frequency for every scale is calculated based on equation 3.4 and the next frequency in the series is $\sqrt{2}$ times the previous one. Feature vector is mean values and standard deviations of magnitudes of filter responses. In order to make the features rotation invariant, the Fourier Transform of the features at seven rotations is calculated and the non-redundant part of power spectrum is used as feature vector. For every tubule, number of features, N_r, are:

$$N_r = N_f N_s (N_o + 1) \tag{4.1}$$

where N_f, and N_s and N_o are respectively number of frequencies, number of scales and number of orientations. In total we have 128 features.

LTP uses a local threshold and the local neighborhood is binarized based on its relation to the threshold. The distribution of the local binary numbers is considered as the feature vector. Binary codes are grouped as one rational group if they can be circularly shifted to the same code. The co-occurrence within rotation groups are Fourier transformed and the non-redundant part of the power spectrum is used as the feature vector. For every pixel we sampled eight points at radius of four and the threshold value is five. We have 652 features.

4.3.3 Classification

For the classification we explored three different classifiers: linear Support Vector Machine, Random Forest and RUSBoost. A soft linear Support Vector Machine (SVM) classifier [18], was trained on a given set

of tubules with known stages. Its parameters was optimized using grid search. 5-fold cross-validation was used to assess the classifier's accuracy. We used LIBSVM package[21] for SVM.

Random Forest [16] is an ensemble classifier method constructed of forest of decision trees. In random forest cross-validation is internally implemented and out of bag error is a good estimate of the general error. We chose 100 trees for the forest.

RUSBoost [77] is designed for imbalanced data set, where RUS stands for random under sampling. It is an ensemble classifier and consists of subsequent week learners. The number of learners used for this application is 200.

4.3.4 Evaluation Using Confusion Matrix

Here we have a multiclass unbalanced classification problem. Accuracy, which is the ratio of correctly classified samples does not give the whole picture of the performance of the classifier. We used a confusion matrix to visualize the classifier results. In confusion matrix (figures 4.3, 4.4 and 4.5), numbers indicate how many tubules were assigned to stage Y (row number) by the pathologist and to stage X (column number) by the computerized staging program, as a percentage of all tubules manually assigned to stage Y. Thus, each row adds up to 100%.

4.4 Results and Discussion

A Pathologist classified 370 sample tubules of four animals into 12 developmental stages. The distribution of tubules for 12 stages are shown in table 4.1. As you can see we have unbalanced data set where some of the stages (e.g. stage 11) are represented with very few examples.

Developmental stages are cyclic and neighboring stages are very similar in structure. It is not an easy task for a pathologist to distinguish some of the neighboring stages with high certainty. On the other hand, we do not have enough samples for every stage. These issues are problematic when training a classifier. We have tested three different classifiers: Random Forest, RUSBoost and SVM for two feature descriptors: LTP and Gabor. The confusion matrices of all results are shown in figure 4.3 and 4.4. None of the classifiers are able to capture the structure of the data for all the stages and are confused between neighboring stages. This problem is more evident in the minority stages. As you can see in confusion matrices in figures 4.3 and 4.4, Random Forest is more biased towards stages one and five which are majority stages whereas RUSBoost is biased towards stages four, seven and eleven which are

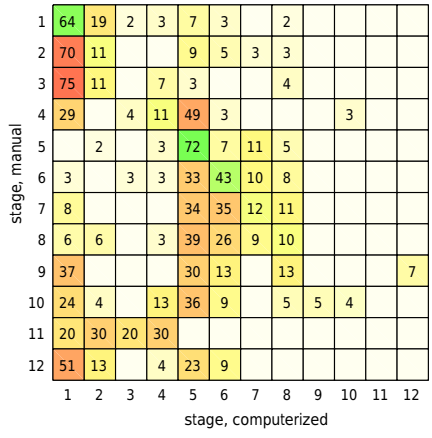

A

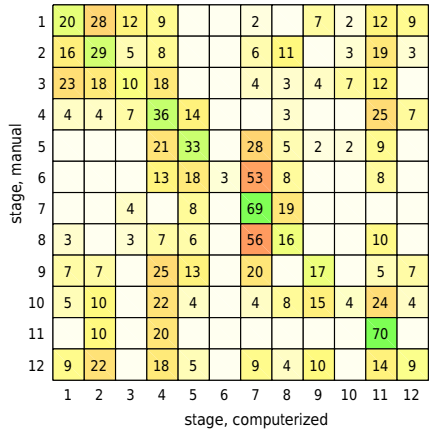

B

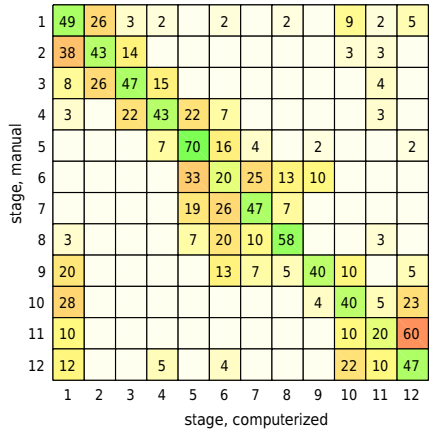

C

Figure 4.3. *Confusion matrices for Gabor features, A is Result of RF, B is result of RUSBoost and C is the result of SVM. Along the diagonal, in shades of green, are the tubules staged identically by the pathologist and the computer program. Other boxes, in shades of red , are tubules where the program did not agree with the pathologist. Empty boxes indicate 0%*

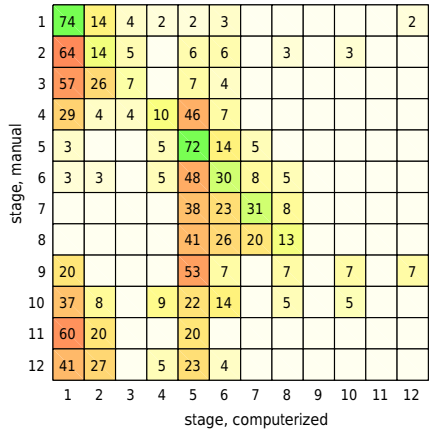

A

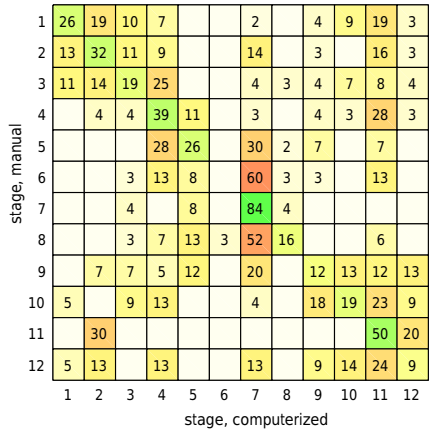

B

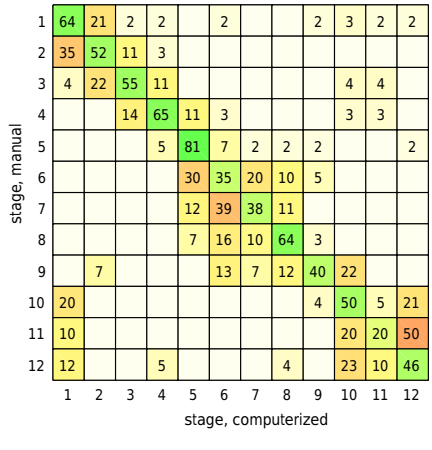

C

Figure 4.4. *Confusion matrices for LTP features, A is Result of RF, B is result of RUSBoost and C is the result of SVM. Along the diagonal, in shades of green, are the tubules staged identically by the pathologist and the computer program. Other boxes, in shades of red, are tubules where the program did not agree with the pathologist. Empty boxes indicate 0%*

Table 4.1. *Distribution of tubules over 12 stages*

stage	count	percent
1	57	15
2	37	10
3	27	7
4	28	8
5	57	15
6	40	11
7	26	7
8	31	8
9	16	4
10	22	6
11	7	2
16	22	6

minority stages. One reason that RUSBoost is biased toward minority class is that it uses the number of the objects in the minority classes and then undersample other classes to makes a balance data set. Undersampled majority classes may not be a good representative of their original classes. Linear SVM for both descriptors perform reasonably well. SVM results are comparable for both Gabor and LTP features. SVM confuses neighboring stages much more frequently than distant stages. This is expected, as the development of spermatids is a continuous process that has been split into stages. The finer the division into stages, the more likely it is that a tubule is close to the boundary between stages, and the more likely it is that neighboring stages are confused.

Pooling of the 12 Stages

Table 4.2. *Distribution of tubules over 5 stages*

stage	count	percent
A	94	25
B	55	15
C	123	33
D	47	13
E	51	14

For better accuracy in classification we can pool stages into fewer number of stages. We suggested pooling of the 12 stages in mink into five different categories (A to E in table 4.2). The new stages (A to E) were chosen based on morphology, but also which stages that are important to evaluate in a toxicological evaluation of the seminiferous

epithelium. Pooling of stages is not new. In rat McClusky et al. [64] pooled the stages into 7 different groups based on the 14 stages defined by Leblond and Clermont [56]. Hess et al. [44], on the other hand, pooled the 14 stages of the rat into four groups.

As we can see in figure 4.5, the performance of classification is better in 5 stage compared to 12 stages and the overall number of correctly classified tubules is 79.6% in this case. Five-stage problem is easier for the computerized staging program can be explained by two main reasons. (1) When grouping tubules into fewer stages, there are more example tubules for each stage, and the classifier is better able to generalize from these examples. (2) When grouping tubules into fewer stages, fewer tubules are close to the boundary between stages, and thus less likely to be confused with neighboring stages.

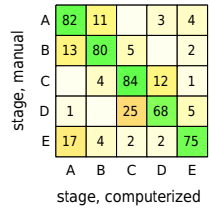

Figure 4.5. *Confusion matrix for 5 stages, for LTP feature and SVM classifier. Along the diagonal, in shades of green, are the tubules staged identically by the pathologist and the computer program. Other boxes, in shades of red , are tubules where the program did not agree with the pathologist. Empty boxes indicate 0%*

4.5 Conclusion

The computerized staging proposed here has a potential to modernize the tedious staging process required in toxicological evaluation of testicular tissue. With whole-slide imaging and automated tubule segmentation in place, the computerized staging program, can be used to efficiently direct the pathologist to tubules of the required stage.

5. Cell type classification and sub-cellular fluorescence quantification in Arabidopsis

5.1 Background

Developmental studies are increasingly focused on the molecular mechanisms that drive differentiation and maturation of stem cells into tissues, organs and organisms. In order to better understand the mechanisms underlying development processes, the study of spatial distribution of molecular factors, which regulate differentiation and determine cell fate, is important. We are interested in study of stem cells and their functionality in wood plant. Stem cells diversify in shape and chemical composition over time in order to meet the functional requirements of wood. To learn about this process, we compare the morphology and chemical composition of these emerging cell types at various developmental stages. Many of these factors can be fluorescently imaged, either through their own inherent fluorescence, via fluorescent fusion proteins, stains, probes, or through immunofluorescence. With the wide range of fluorescence tools, Laser Scanning Confocal Microscopy (LSCM) has become the method of choice to localize and quantify developmental makers. Fluorescent imaging of morphogen gradients in the Drosophila embryo and of auxin transport proteins in the Arabidopsis shoot and root tip have, for example, greatly contributed to our understanding of pattern formation and development [40, 50]. Fluorescent images of Hypocotyl and stem are shown in figure 5.1. Stem cells in hypocotyl and stem differentiate into several cell types of the xylem (inner tissue) and phloem (outer tissue) [47].

The distribution of determinants of differentiation and development over larger spatial ranges of tissues is often more relevant than localization of the signal within a single cell. Thus, such analyses typically involve thousands of nuclei or cells. Nevertheless, many of these studies rely on comparison of fluorescence intensity between manually defined regions of interest (ROIs) e.g. between different cell types. Obviously, manual segmentation into ROIs is labor-intensive and underlies human subjectivity and inconsistency that may severely limit the interpretability of LSCM data. Recent advances in image acquisition and analysis, together with improvements in microprocessor performance, have

brought automated methods within reach. Computer-assisted quantification of fluorescent targets on a cellular scale over large spatial ranges requires both accurate automatic segmentation and quantification of fluorescence in each individual segment [43].

Here, we provide an image analysis pipeline: 1) segment radial plant organs into individual cells from cell wall specific stain, 2) to classify cells into categories based upon Random Forest classification, 3) to divide each cell into sub-regions, and 4) quantify fluorescence intensity to a sub-cellular degree precision for a separate fluorescence channel. In this study, we demonstrate the precision of this analytical process for the relatively complex tissues of Arabidopsis hypocotyls at various stages of development. High speed and robustness make our approach suitable for large data sets and other tissue types.

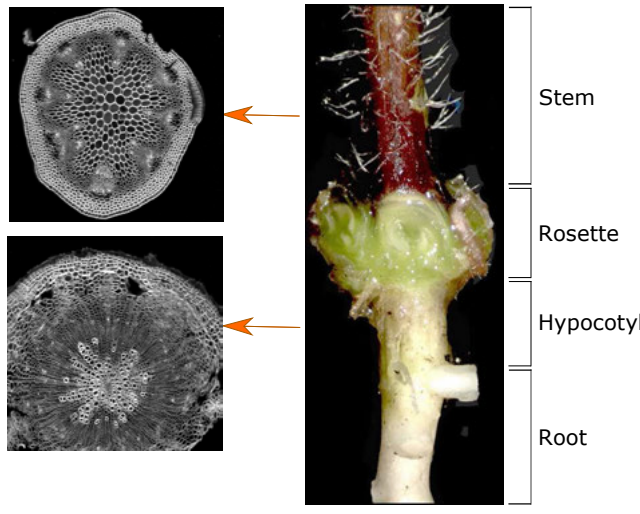

Figure 5.1. *Fluorescent images of hypocotyl and stem of Arabidopsis plant.*

5.2 Materials and Imaging

Hypocotyl sections were imaged using a confocal laser scanning microscope with a 10x, 0.45 NA plan-apochromat objective lens. The field of view was adjusted slightly for each specimen to encompass all relevant areas of the sample and maximize sampling density. Resulting images were 1024 x 1024 pixels, with a pixel width and height 0.8 μm.

5.3 Algorithm

5.3.1 Segmentation

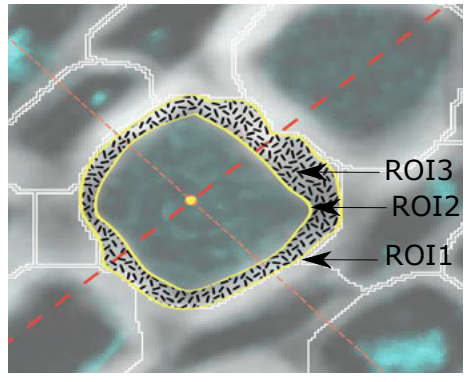

Figure 5.2. *Three regions of interests ROI1: the whole cell , ROI2: the cell lumen, ROI3: cell wall.*

There are three different regions of interest (ROIs) to segment. The whole cell, the cell wall and the cell lumen (figure 5.2). We used Watershed segmentation to delineate the cells borders. In order to have a good segmentation result using Watershed every region of interest, here cells, should have one minimum. The original images are noisy and we first used Gaussian filter with variance 1 pixel to remove noise. Then we applied Watershed. In some cells we have oversegmentation. We merged regions where the intensity difference between their minimum and the value of the first pixel on dam touching the two regions is less than 10. The lumen boundary within each watershed region was precisely identified using Otsu's thresholding algorithm [71]. The walls are the result of subtraction of the cells from their lumens.

5.3.2 Feature Description

As you can see in figure 5.4, cells are different in terms of morphology, location, orientation and amount of fluorescence they absorb. We measured features based on these differences. All the features are shown in table 5.1.

The eccentricity in table 5.1 is defined as follows:

$$e = \sqrt{\frac{1 - L_1^2}{L_2^2}} \tag{5.1}$$

Table 5.1. *Features extracted from ROIs*

Morphology features for every cell
Area, perimeter, radius, product of lengths of major and minor axes of the cell, eccentricity (equation 5.1), P2A (equation 5.2), length of major axis of cell.
Location and orientation based features
Radial coordinate of cell center, origin at center of tissue, Angular coordinate of cell center, origin at center of tissue (θ_1), The angle between major axis and horizontal axis (θ_2), Acute angle between radial vector of cell and major axis of cell (θ_3) (see figure 5.3)
Fluoresce based feature
Median of cell intensity, mean of cell intensity, median of cell wall intensity, mean of cell wall intensity

where L_1 is the length of minor axis and L_2 is the length of major axis of the object. P2A in table 5.1 is defined as follows:

$$\text{P2A} = \frac{p^2}{4\pi a} \tag{5.2}$$

where p is the perimeter and a is the area of the object.

In total we have 18 features. Some of the features are correlated and using all of them has undesired effect on classification result. We need to select the features that give the best classification result. The naive search algorithm considers all subsets and is a very expensive approach. Instead we followed a heuristic approach, that yields a good combination of features, though not necessarily the best. We started with a few features that intuitively seemed important, then added features one at the time and compared classification performances. At the end, we selected five features: the radial coordinate of cell center, area, acute angle between the radial vector of the cell and the major axis of the cell (θ_3), median of the cell intensity, and median of the cell wall intensity.

5.3.3 Classification and Evaluation

We used supervised classifiers. For supervised classification we need training data which consist of example cells from different classes. A biologist manually labeled six different cell types in 21-day old hypocotyls (figure 5.4). For each class, cells were chosen that best represented the

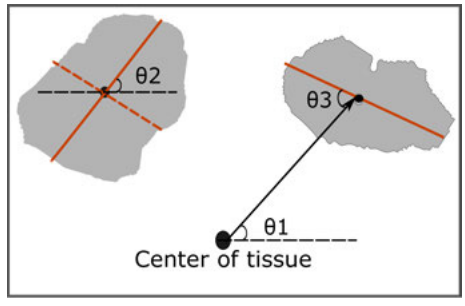

Figure 5.3. *Red lines are major and minor axis of cells. Radial vector is defined as the vector between center of tissue and center of cell, shown as black arrow.*

class, avoiding selection of cells that lay on vague boundaries between cell types or exhibited morphology that were intermediate between cell classes. Cells were chosen from four different images and in total we have 1270 training cells. We have 240 samples for every class except for phloem fibers (yellow cells in figure 5.4) of which we have 70 samples. Phloem fibers are generally represented few times in an image.

For the classification we tested three different classifiers: linear Support Vector Machine (SVM), non-linear SVM [18] and Random Forest [16]. Random Forest is an ensemble classifier method constructed of forest of decision tree. We chose 100 trees for the forest. SVM parameters were optimized using grid search. For the evaluation, we used 5-fold cross-validation on the training set and calculated the average of 5 confusion matrices. We also applied the classifiers on all the cells in the images and an expert evaluated the results.

5.4 Result and Discussion

We applied Watershed and Otsu's thresholding method to segment cells, and their lumens. The result of the segmentation is shown in figure 5.5. The cells are then divided to four sub-regions (figure 5.5). Sub-region-specific ROIs provide a high resolution measurement of fluorescence distribution.

The segmentation method works very well on majority cells of an image. We applied three classifiers: Linear SVM, non-linear SVM (with radial basis function) and Random Forest. We used 5-fold cross-validation for evaluation. The confusion matrix is the average of confusion matrices of all the 5 folds. For SVM methods, parameters were optimized using grid search. The confusion matrix of three classifiers is shown in figure 5.6. Non-linear SVM has the worst result. Linear SVM and Random Forest both work well and their results are comparable. Non-linear SVM has a difficulty on detecting minority class (class 4 which is pholem

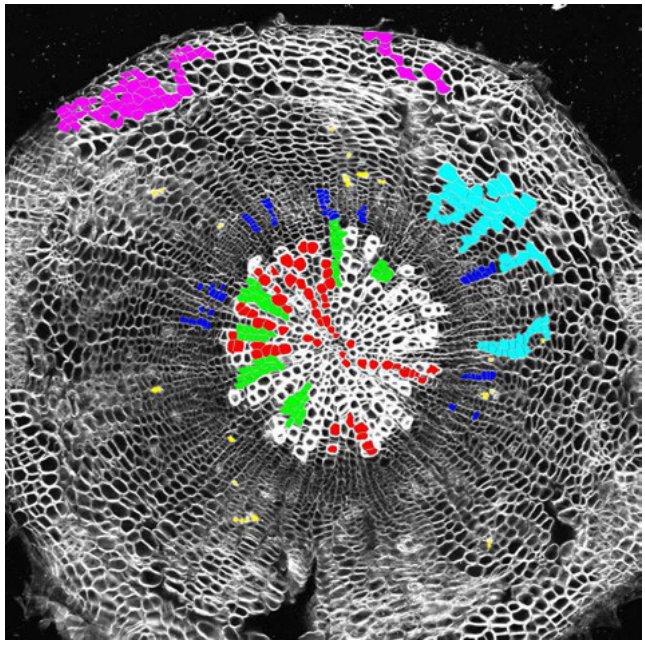

Figure 5.4. *Training set for 21-day old (dag) hypocotyls: xylem vessels (red) and parenchyma (green), cells of the cambial zone (dark blue), phloem fibers (yellow), phloem (blue), cortical cells (purple).*

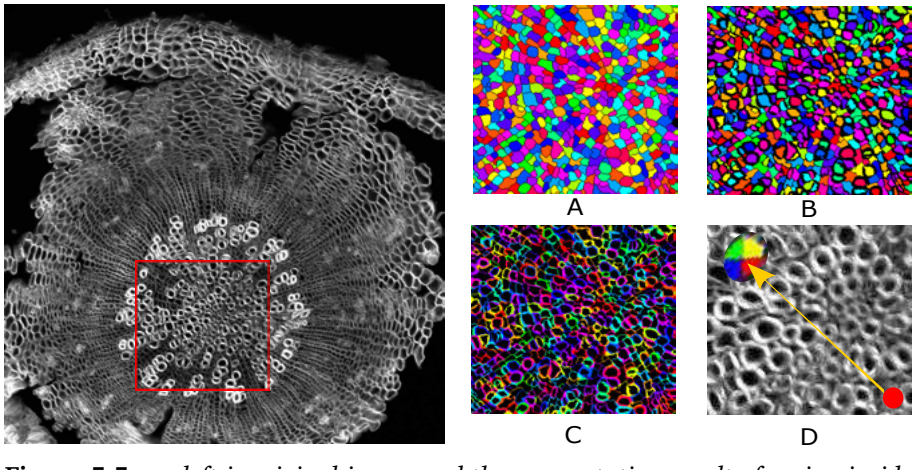

Figure 5.5. *on left is original image and the segmentation result of region inside red box is shown on right. A: segmented cells, B: segmented lumens, C: segmented walls, D: sub-cell division. yellow arrow in D is the vector from center of tissue (red dot) to center of cell.*

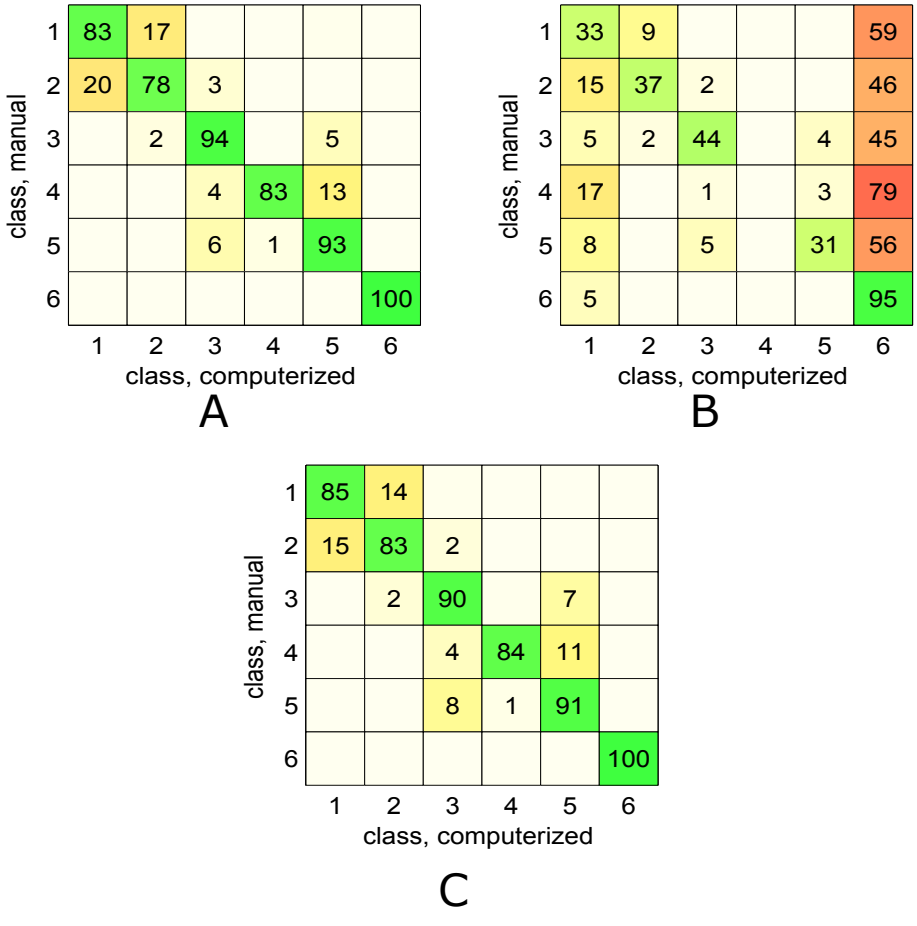

Figure 5.6. *Confusion matrix for the three different classifiers, A: linear SVM, B: SVM with radial basis function, C: Random Forest. 1:xylem vessels, 2: parenchyma, 3: cells of the cambial zone, 4: phloem fibers, 5: phloem, 6: cortical cells. Numbers indicate how many cells were assigned to class Y (row number) by a biologist and to class X (column number) by the computer program, as a percentage of all cells manually assigned to class Y. Thus, each row adds up to 100%. Along the diagonal, in shades of green, are the cells classified identically by the biologist and the computer program. Other boxes, in shades of red , are cells where the program did not agree with the biologist. Empty boxes indicate 0%*

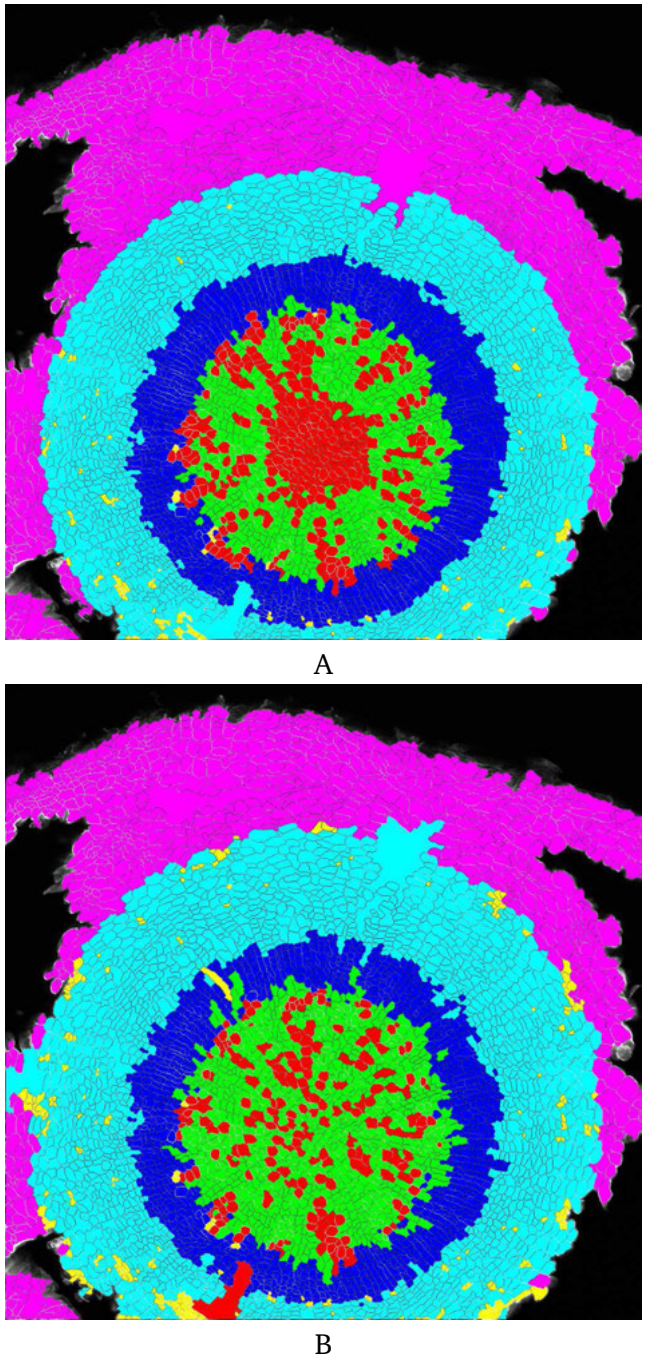

A

B

Figure 5.7. *Classification results, A: Random Forest, B: linear SVM.*

fiber) and is more biased toward class 1 (xylem vessels) and 6 (cortical cells). The location of the cells which plays a main role in manual cell classification does not play the same role in non-linear SVM classifier.

In every image we have around 5000 cells and for all images we have a few hundred thousand of cells. In the training set we have only 1270 cells which is not enough to capture all the variations of the cells. Considering this point, the estimate of performance of classifiers by cross-validation on the training set may not be trustworthy. We applied the classifiers on the whole cells of an image and a biologist expert evaluated the result. The result of linear SVM and Random Forest are shown in figure 5.7. As we can see in this figure, linear SVM cannot distinguish between xylem vessels and parenchyma while Random Forest is doing a better job in classifying them correctly. Also Random Forest can recognize minority class (class 4, phloem fibers) better.

We chose Random Forest as the classifier. As an output of Random Forest we also have posterior probability for every cell. We can use this value to remove cells with low probability, where the classifier is not confident about their labels.

With robust, accurate classification, each ROI (and sub-ROI) provides a mask to conduct a variety of measurements of fluorescence. For the purpose of demonstration, we probed tissues with an antibody specific to xylem in the secondary cell wall. A fluorescent secondary antibody permitted visualization of epitope localization. In 21 dag hypocotyls, secondary cell walls occur exclusively in the xylem vessels, thereby providing a clear case of cell type-specific fluorescence to validate the quantification methodology. We measured the average value of wall intensity (wall signal) in every cell. Comparison of the fluorescence channel (figure 5.8B) with a spatial mapping of the ROI values for wall signal (figure 5.8C) demonstrates that the quantification replicates the source fluorescence image, although entire cells are filled-in since the display methodology does not color walls discretely.

As proof-of-concept that the classification provides a meaningful basis to group cells for fluorescence characterization, we next examined the means of wall signal values for all cells of each cell class, filtering at 50, 70, and 90% (figure 5.8G). From figure 5.8G, it is clear that the xylem vessels are the dominant cell type that exhibit a fluorescence signal. Not evident with visual examination of the spatial map of wall signal (figure 5.8C), the xylem parenchyma exhibit signal. Where a vessel and a parenchyma are neighbors, the thick wall of the vessel gets split into two by the Watershed segmentation. Also the pixels given as boundary by the Watershed segmentation method are assigned to both neighbors when doing the measurement. These two issues can be primary causes of signal bleed into parenchyma cells.

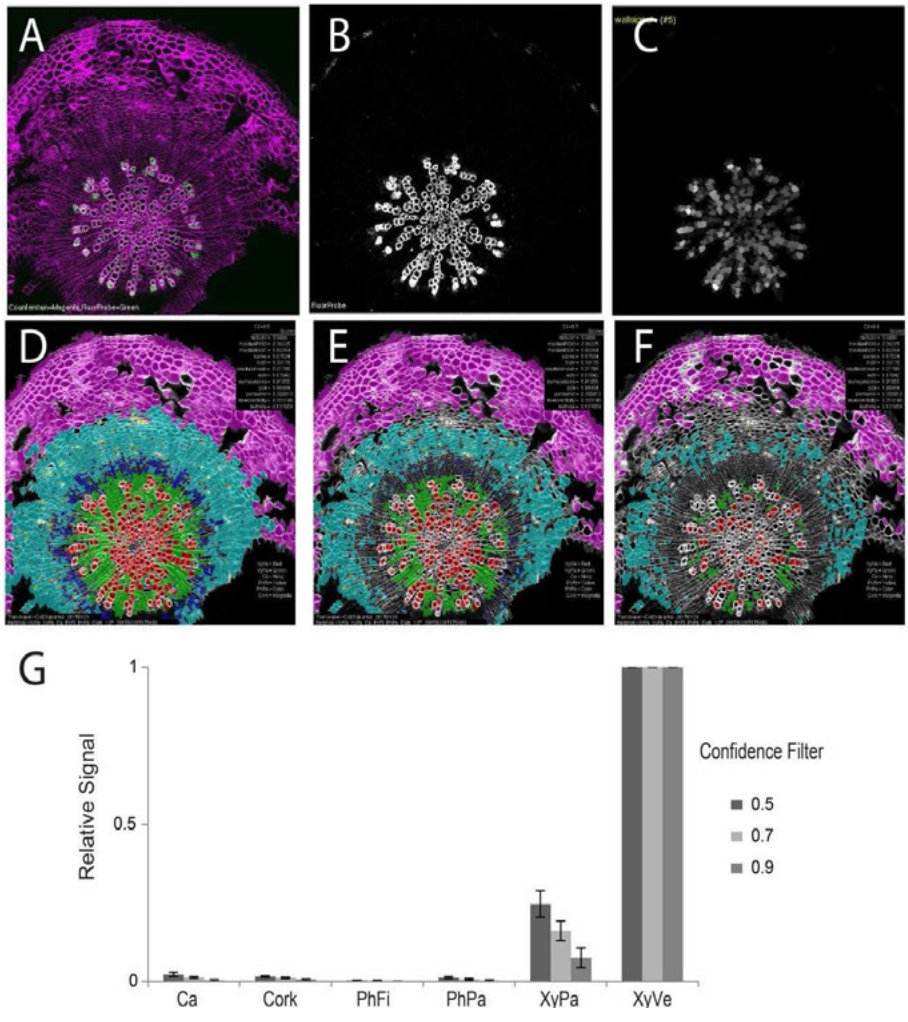

Figure 5.8. *Quantification of second channel (fluorescence) for a representative tissue (21-day-old wild-type hypocotyl) labeled with xylem-specific antibody (LM10). A) Overlay image of CFW counterstain channel (magenta) and LM10 immunolabel (green) channel. B) Isolated immunolabel channel after background fluorescence correction. C) Wall signal for ROIs objects. Classification result and relative wall signal for 50 (D), 70 (E) and 90% (F) confidence filtering. G) Quantification of relative fluorescence intensity. Error bars represent the standard deviations of relative signal intensities.*

5.5 Conclusion

We suggested a data analysis pipeline that efficiently and accurately provides a wealth of morphometric data for automatically categorizing cell types of transverse sections of Arabidopsis hypocotyls. Furthermore, our pipeline provides a robust means to accurately quantify immunofluorescence for specific cell types, filterable by confidence scores for individual cells.

6. Conclusions and Future Work

This chapter concludes the thesis and presents some directions for future work.

6.1 Summary of Contributions

I developed two automated analysis pipelines for two rather different applications. All developed methods in image processing have some parameters that need to be tuned and tailored based on application data. Although many of these methods have a rich mathematical foundation, they also make many assumptions that may not hold in real applications. Complicated structure and huge variation of data in biology data make developing a fully automated pipeline a very hard task. I have developed pipelines that can work well on two complicated applications and both have generalization property.

The first pipeline I developed is for histopathological analysis of testicular tissue, which could be used in toxicological research. To segment tubular structure in testicular tissue, I suggested two automated methods for two different stainings. For Periodic Acid Schiff (PAS) stained thin sections, I first delineate the border of the lumen using the Level set method. The border of the tubules are then segmented using a thresholding method followed by an approach based on geodesic distance to correct under-segmentation. For Gata-4 antibody staining, the cell nuclei are first detected using the fast radial symmetry filter. A graph is constructed on top of the epithelial cells, then a Graph cut segmentation method is used to cut the links between the cells of different tubules. To classify tubules in twelve different stages, I used texture descriptors based on the local ternary patterns, and applied a linear support vector machine for the classification. In the 5 stage case, the overall number of correctly classified tubules is 79.6%.

The second pipeline I developed is for quantification of gene expression in the various cell and tissue types in plant organisms. In order to better understand the mechanisms of the underlying development processes, it is important to study the spatial distribution of molecular factors, which regulates the differentiation and determines the cell fate. The segmentation of cell structures in the tissue is necessary for quantitative and qualitative assessment of the gene expression. The

classification of segmented cells further provides the ability to generate chemical profiles of specific cell types. I segmented the cells using the Watershed method. A range of feature descriptors based on morphology, intensity, location and orientation of cells were defined. A Random Forest classifier was used to classify cells into the different types in the xylem (inner tissue) and phloem (outer tissue).

6.2 Future perspectives

The latest advances in digital cameras combined with powerful computer software enabled us to store high quality images of specimen from microscopy. The field of quantitative image analysis has steadily gained relevance within the bio-medical sciences. Due to large variety of imaging techniques and tissue preparation methods, there are many research challenges in automating the analysis of data for different types of applications. It is important to develop a pipeline with components that are simple enough to be generalized and have predictive value. Considering huge variation in the available data set, designing such an algorithm is one of the biggest challenges in the field of medical image processing.

Automated segmentation method

The first and most challenging step in an image analysis pipeline is segmentation. In order to have a fully automated method, we need to develop a segmentation technique that can segment regions of interest in the image without user intervention. The general assumptions in image segmentation methods is that the pixel intensity in objects are coherent and distinct from the background or that the object has a clear border. Such assumptions are difficult to meet in complicated histology images. In the histology images of testicular tissue, the complex structure of tubules and their weak border made the segmentation of tubules very challenging. I suggested two automated methods for two different staining techniques. They both worked well on the available data set but still need improvement to be more general and robust. The plant cells in florescent images had simpler structure and the suggested segmentation method can detect ROIs with great accuracy.

Ground Truth

In order to evaluate different steps of an algorithm, we need a trustworthy ground truth. Large differences between data sets in biological applications prohibit fair comparison of performance, reliability and accuracy of proposed methods. In order to develop an algorithm, we need

experts' opinions to evaluate its performance. For complicated data, experts frequently do not agree [27, 59]. Establishing a rich ground truth data set with the help of many biologist experts can assist in developing a more accurate algorithm. This can also help in reproduciblity of experimental results. Unfortunately availability of such data is limited. The proposed pipelines can definitely benefit from such data in terms of performance and generalization.

6.3 Conclusion

As discussed, the generalization property of an automated algorithm is very important. Complex algorithms with many parameters may ultimately lead to a better outcome in a specific data set, however at the same time it can harm the generalization property of algorithm. Fewer assumptions on the characteristics of the data can increase the predictability of the algorithm. Medical images, such as histopatolgy images and florescent images of plant cell are complicated and using complex algorithms is inevitable. However it is important to keep the effect of the parameters that influences the output as minimal as possible. In both pipelines we considered these issues.

Although developing a fully automated method is attractive, sometimes having some sort of interaction with the user can help in simplifying the pipeline and improve accuracy. Developing a semi-automated pipeline that can generate correct results in a reasonable time can also be an option.

Summary in Swedish

De senaste förbättringarna av digitala kameror tillsammans med kraftfull programvara gjorde det möjligt för oss att skapa mikroskopibilder av vävnad av hög kvalitet. Att analysera hundratals bilder manuellt tar mycket lång tid och dessutom blir det problem med mänsklig subjektivitet och inkonsekvens. Kvantitativ bildanalys är ett område på frammarsch som är på väg att börja tillämpas på mikroskopibilder vid kliniska forskningscentra. Eftersom bilderna kan skapas på många olika sätt och eftersom det också finns många olika sätt att preparera vävnad så finns det också många utmaningar när det gäller automatisering av analysen inom olika tillämpningsområden. Det är viktigt att utveckla en serie operationer, en pipeline, vars komponenter är enkla nog att kunna generaliseras och som är prediktiva. Eftersom variationerna i de tillgängliga datamängderna är mycket stora är en av de största utmaningarna inom medicinsk bildanalys att designa sådana algoritmer. Den här avhandlingen behandlar automatisering av kvantitativ analys av vävnad i två olika tillämpningar: patologi och växtbiologi.

Testikelvävnad har en komplex struktur, den består av tubformade sädeskanaler, tubuli. Sädeskanalernas epitel innehåller celler som omvandlas från primitiva könsceller till spermier i ett antal steg. Hos minken kombineras de olika stegen till tolv stadier. The society of toxicological pathology rekommenderar att testikelns epitel klassificeras som dessa olika stadier vid utvärdering av vävnadsskador för att avgöra om spermatogenesen har blivit störd. Avhandlingen presenterar automatiska metoder för snabb och robust segmentering och klassificering av tubulistrukturer. Vi föreslår segmenteringsmetoder för två olika infärgningsmetoder. För Periodic Acid-Schiff (PAS) infärgning av tunna snitt hittar vi först kanterna på lumi na med en level-set metod. Tubernas kanter segmenteras fram med tröskling, vilket följs av en metod baserad på geodetiska avstånd för att korrigera översegmentering. För GATA4 antikroppsinfärgning detekteras först cellkärnorna med ett snabbt radiellt symmetrifilter. En graf konstrueras sedan över epitelcellerna och efter detta används en grafsnittsmetod för att bryta länkarna mellan celler från olika tubuli. Nästa steg är att hitta särdrag som karakteriserar informationen från varje tubulus. Patologer undersöker tubuli lokalt, baserat på de celltyper de innehåller, och tilldelar dem ett stadium. Texturdeskriptorer fångar de spatiala förhållandena mellan pixlar. Tubuli som innehåller olika celltyper har också olika textur. Vi utnyttjar två

texturdeskriptorer: Gabor-filter och Lokala Ternära Mönster (LTP). LTP använder en lokal tröskel och den lokala omgivningen binäriseras baserat på dess relation till tröskelvärdet. De binära talen omvandlas till decimaltal och dessas histogram används som särdragsvektorer. Gaborfilter är en samling filter med olika skala, orientering och frekvens. Bilden filtreras med samtliga filter och sedan används medelvärde och standardavvikelse för filtersvaren som särdragsvärden. För klassificeringen använde vi tre olika klassificerare: stödvektormaskin (SVM), Random Forest och Rusboost. Random Forest och Rusboost är ensembleklassificerare. Rusboost är designad för obalanserade datamängder, där RUS betyder Random Under Sampling. Den undersamplar majoritetsklassen och använder AdaBoost för träning. Av de olika möjliga kombinationerna av dessa algoritmer fungerar LTP tillsammans med SVM bäst. Den träningsdatamängd som tillhandahölls av patalogen är obalanserad: vissa stadier är starkt representerade medan andra är sällsynta. Anledningen till att detta är ett problem är att klassificerare som inte tar hänsyn till den här obalansen troligen snedvrider resultaten och överrespresenterar de vanligaste stadierna. I klassificeringsresultaten ser vi också en stark korrelation mellan andelen tubuli som klassas som korrekt stadium och antalet exempel på detta stadium. Klassningsresultaten blir alltså inte tillfredställande för de ovanliga stadierna. För att få bättre noggrannhet och statistisk analys föreslog vi att slå samman stadierna och minska antalet från tolv till fem tydliga stadier. Sammanslagningen baseras på tubuliernas morfologi. Med fem stadier klassas 79.6% av tubuli korrekt. Om avbildning av hela objektglaset och automatisk segmentering av tubuli fungerar kan det datoriserade klassificeringsprogrammet som presenteras här användas för att effektivt visa patologen på tubuli i det begärda stadiet.

Kontextuell information för var flourescens förekommer i mikroskopibilder av växtdelar hjälper oss att bättre förstå differentiering och omvandling av stamceller till olika vävnadstyper. Förändringar i morfologi och cellväggssammansättning indikerar graden av differentiering och celltyp. Att segmentera celler och klassificera dem som olika celltyper gör det möjligt att utföra statistisk analys och kvantifiering av en viss celltyp. Vi segmenterar cellerna med vattendelarmetoden (watershed). Ett antal särdrag baserade på morfologi, intensitet, läge och orientering av cellerna definierades. Random Forest-klassificering och SMV testades på datamängden. Random Forest fungerade bäst när det gällde att klassificera olika typer av celler i xylem (inre vävnad) och floem (yttre vävnad). Med robust och noggrann klassificering av varje cell (och celldel) kan vi utföra ett antal olika mätningar av flourescens i varje cell och celltyp. För att visa att klassificeringen grupperar cellerna på ett meningsfullt sätt för att sedan kunna karakterisera deras flourescens använde vi en antikropp som binder till xylems sekundära cellvägg.

Mätningar av flourescensens intensitet i olika cellklasser enligt vår metod visar tydligt att xylemkärlen är den celltyp som avger mest flourescens.

Acknowledgements

I would like to extend my sincere gratitude to all those people who contributed in this thesis directly or indirectly. This would not have been possible without their generous support and encouragement.

- **Cris Luengo**, my main supervisor to whom I owe a huge debt of gratitude. His dedication and enthusiasm for scientific research and his insight have been inspiring. It was a great honor for me to collaborate with him in various projects. Thank you for believing in me and making my Ph.D. studies a rewarding experience.
- **Gunilla Borgefors**, my co-supervisor, for her great insight in research and offering me valuable advice. Thank you for teaching me to be always persistent in achieving my goals.
- **Lena Holm**, my co-supervisor, for her valuable support during my Ph.D. studies.
- **Ellinor Spörndly-Nees**, for the long and enjoyable collaboration and for introducing the world of histopathology to me. Thank you for all nice fikas and dinners we had together
- **Hardy Hall**, **Urs Fischer**, **Elisabeth Ekstedt** and **Abdolrahim Kadkhodamohammadi**, for excellent collaborations and scientific discussions to the themes of research in this thesis.
- **Ingela Nyström**, the VI2 division head, for taking care of us in the best way possible.
- **Lena Nordström**, for keeping the whole system running. Thank you for the delicious grape and cheese snacks.
- **Ida-Maria Sintorn**, **Ingrid Carlbom**, **Carolina Wälhby** and **Natasa Sladoje**, for the great scientific, career and life advice.
- **Gustaf Kylberg**, my colleague and friend for answering all my questions in great detail as promptly as he could. Thank you for generously sharing your knowledge in the field of texture analysis with me.
- **Vladimir Curic**, my colleague and friend, for sharing all his great experience as a senior Ph.D. student with me and for offering help whenever I needed. Thank you for introducing me to different cuisines in Uppsala.
- **Kristina Lidayova** and **Christophe Avenel**, my officemates, for creating a great atmosphere for both working and having fun.

- **Elisabeth Linnér**, for sharing her interesting perspective of life with me. Thank you for your care and support in difficult times.
- **Pontus Olsson**, for always having a smile on his face and sharing positive energy.
- **Lennart Svenson**, **Hamid Sarve**, **Johan Nysjö** and **Fredrik Nysjö**, for their friendship and for nice lunches we had together.
- **Andreas Kårsnäs**, for making my summer school trip to Burno and the MICCAI Conference trip to Toronto a memorable time for me.
- **Jimmy Azar**, for sharing his pattern recognition expertise, by giving an excellent course in pattern recognition. Thank you for fun discussions.
- **Bahareh Fakhrzadeh**, **Somayeh Azarnoush**, **Mahtab kamali**, **Narges Simjour** and **Masoomeh Rudafshani** for helping me get through the difficult times. Thank you for all the emotional support.
- I would like to thank my friends in Uppsala who made my life here a wonderful experience: **Mojataba Solatanalian**, **Azadeh Haghighi**, **Elham Roshan**, **Sobhan Badiozamany**, **Narges Rajabnezhad**, **Javad Bakhshi**, **Serveh Karimi** and **Rahim Kadkhodamohammadi**. Thank you for nice Persian dinners.
- **Majed Ashoorioon**, for manual segmentation and for encouraging me to be active and do more physical activity.
- **Hassan Fakhrzadeh**, my late grandfather, for always encouraging me to follow my dreams and be strong.
- My sister **Faezeh**, for being there when I needed her the most. Thank you for always keeping me updated with all family's news. I would like to thank, my brother **Mohammad** for his sense of humor and all rides he gave to me during my visits to Iran and my sister in law **Sara** for her kindness.
- My dear mother **Ashraf**, and my dear father **Mehdi**, who stood by me in every decision I made in life. Certainly, without their care and support, I would have not been able to achieve what I did.
- I would like to thank my bundle of joy, for sharing every moment of writing this thesis with me. Thank you for your patience, we made it together! I am looking forward to see your beautiful face.
- **Amjad**, my husband and very best friend, for encouraging me to apply for this Ph.D. position. His passion for science and research is always inspiring for me. We accomplished a lot together and I hope we continue as such. Thank you for your faithful support and being my source of strength when I could not find my own. I love you! ♡

References

[1] A. Lytwyn A, I. E. Salit, J. Raboud, W. Chapman, T. Darragh, B. Winkler, J. Tinmouth, J. B. Mahony JB, and M. Sano. Interobserver agreement in the interpretation of anal intraepithelial neoplasia. *Cancer*, 103: 1447–1456, 2005.

[2] Madabhushi A. Digital pathology image analysis: opportunities and challenges. 2009.

[3] W.C. Jr. Allsbrook, K. A. Mangold, M. H. Johnson, R. B. Lane, C. G. Lane CG, and J. I. Epstein. Interobserver agreement in the interpretation of anal intraepithelial neoplasia. *Human Pathology*, 32(1):81–88, 2001.

[4] S. Arivazhagan, V. L. Ganesan, and S. P. Priyal. Texture classification using gabor wavelets based rotation invariant features. *Pattern Recognition Letters*, 27(16):1976–1982, 2006.

[5] William A. Barrett and Eric N. Mortensen. Interactive live-wire boundary extraction. *Medical Image Analysis*, 1:331–341, 1997.

[6] P. Bassan, As. Sachdeva, J. H. Shanks, M. D. Brown, N. W. Clarke, and P. Gardner. Automated high-throughput assessment of prostate biopsy tissue using infrared spectroscopic chemical imaging. *Proceedings of SPIE*, 9041:90410D–90410D–10, 2014.

[7] N. Basu, A.M. Scheuhammer, S.J. Bursian, J. Elliott, K. Rouvinen-Watt, and H.M. Chan. Mink as a sentinel species in environmental health. *International Journal of Environmental Research and Public Health*, 103: 130–144, 2007.

[8] S. Beucher and C. Lantuejoul. Use of watersheds in contour detection. *International Workshop on Image Processing: Real-time Edge and Motion Detection/Estimation, Rennes, France*, 1979.

[9] S. Beucher and F. Meyer. *The morphological approach to segmentation: the watershed transformation*. E. R. Dougherty, Edited by Marcel Dekker, New York, 1993.

[10] F. Bianconi and A. Fernndez. Evaluation of the effects of gabor filter parameters on texture classification. *Pattern Recognition*, 40(12): 3325–3335, 2007. doi: http://dx.doi.org/10.1016/j.patcog.2007.04.023.

[11] F. Bianconi, A. Fernàndez, and A. Mancini. Assessment of rotation-invariant texture classification through gabor filters and discrete fourier transform. *Proceedings of the 20th International Congress on Graphical Engineering*, 2008.

[12] B. E. Boser, I. M. Guyon, and V. N. Vapnik. A training algorithm for optimal margin classifiers. *Proceedings of the 5th Annual ACM Workshop on Computational Learning Theory*, pages 144–152, 1992.

[13] Y. Boykov and G. Funka-Lea. Graph cuts and efficient n-d image segmentation. *International Journal of Computer Vision*, 70(2):109–131, 2006.
[14] Y. Boykov and V. Kolmogorov. An experimental comparison of min-cut/max-flow algorithms for energy minimization in vision. *IEEE Transactions on Pattern Analysis and Machine Intelligence.*, 26(9): 1124–1137, 2004.
[15] Y Boykov, O Veksler, and R. Zabih. Optimal approximation by piecewise smooth functions and associated variational problems. *IEEE Transactions on Pattern Analysis and Machine Intelligence*, 23(11):1222–1239, 2001.
[16] L. Breiman. Random forests. *Machine Learning*, 45(1):5–32, 2001.
[17] L. Breiman, J. Friedman, R. Olshen, and C. Stone. *Classification and Regression Trees*. Wadsworth and Brooks, Monterey, CA, 1984.
[18] C. J. C. Burgess. A tutorial on support vector machines for pattern recognition. *Data Mining and Knowledge Discovery*, 2(2):121–167, 1998.
[19] V. Caselles, R. Kimmel, and G. Sapiro. Geodesic active contours. *International Journal of Computer Vision*, 22(1):61–79, 1997.
[20] T. Chan and L. Vese. Active contours without edges. *IEEE transactions on image processing*, 10(2):266–277, 2001.
[21] C. C. Chang and CH. J. Lin. LIBSVM: A library for support vector machines. *ACM Transactions on Intelligent Systems and Technology*, 2(3): 27–27, 2011. Software available at `http://www.csie.ntu.edu.tw/~cjlin/libsvm`.
[22] N.V. Chawla, K. W. Bowyer, L. O. Hall, and W. P. Kegelmeyer. Smote: synthetic minority over-sampling technique. *Journal Of Artificial Intelligence Research*, 16:321–357, 2002.
[23] A. Chodorowski, U. Mattsson, M. Langille, and G. Hamarneh. Color lesion boundary detection using live wire. *Medical Imaging: Image Processing*, 5747(1):1589–1596, 2005.
[24] L. D. Cohen. On active contour models and balloons. *Computer Vision, Graphics, and Image Processing: Image Understanding*, 53(2):211–218, 1991.
[25] C. Cortes and V. Vapnik. Support-vector networks. *Machine Learning*, 20 (3):273–297, 1995.
[26] E. Cosatto, M. Miller, H. P. Graf, and J. Meyer. Grading nuclear pleomorphism on histological micrographs. *19th International Conference on Pattern Recognition*, pages 1–4, 2008.
[27] M. Costantini, S. Sciallero, A. Giannini, B. Gatteschi, P. Rinaldi, G. Lanzanova, L. Bonelli, T. Casetti, E. Bertinelli, O. Giuliani, G. Castiglione, P. Mantellini, C. Naldoni, P. Bruzzi, and for the SMAC Workgroup. Interobserver agreement in the histologic diagnosis of colorectal polyps: the experience of the multicenter adenoma colorectal study (smac). *Journal of Clinical Epidemiology*, 56(3):209–214, 2003.
[28] J. Cousty, G. Bertrand, L. Najman, and M. Couprie. Watershed cuts: Minimum spanning forests and the drop of water principle. *IEEE Transactions on Pattern Analysis and Machine Intelligence*, 31(8): 1362–1374, 2009.

[29] D. M. Creasy. Review article: Evaluation of testicular toxicity in safety evaluation studies: The appropriate use of spermatogenic staging. *Toxicologic Pathology*, 25(2):119–131, 1997.
[30] D. M. Creasy. Evaluation of testicular toxicology: a synopsis and discussion of the recommendations proposed by the society of toxicologic pathology. *Birth Defects Res B Dev Reprod Toxicol*, 68(5):366–367, 2003.
[31] P. Díaz-Gimeno, M. Ruiz-Alonso, D. Blesa, N. Bosch, J.A. Martínez-Conejero, P. Alamà, N. Garrido, A. Pellicer, and C. Simón. The accuracy and reproducibility of the endometrial receptivity array is superior to histology as a diagnostic method for endometrial receptivity. *Fertility and Sterility*, 99(2):508–517, 2013.
[32] T. G. Dietterich, R. H. Lathrop, and T. Lozano-Perez. Solving the multiple instance problem with axis-parallel rectangles. *Artificial Intelligence*, 89(1-2):31–71, 1997.
[33] E. W. Dijkstra. A note on two problems in connexion with graphs. *Numerische Mathematik*, 1:269–271, 1995.
[34] S. Doyle, M. Hwang, K. Shah, A. Madabhushi, J. Tomaszewski, and M.Feldman. Automated grading of prostate cancer using architectural and textural image features. In *IEEE International Symposium on Biomedical Imaging (ISBI)*, pages 1284–1287, 2007.
[35] A.X. Falcao and J. K. Udupa. User-steered image segmentation paradigms: Live wire and live lane. *Graphical Models and Image Processing*, 60(4):233–260, 1998.
[36] R. A. Fisher. The use of multiple measurements in taxonomic problems. *Annals of Eugenics*, 7(2):179–188, 1936.
[37] I. Fogel and D. Sagi. Gabor filters as texture discriminator. *Biological Cybernetics*, 61(2):103–113, 1989.
[38] Y. Freund and R. E. Schapire. A short introduction to boosting. *Transactions of the Japanese Society for Artificial Intelligence*, 14(5): 771–780, 1999.
[39] L. Grady. Random walks for image segmentation. *IEEE Transactions on Pattern Analysis and Machine Intelligence*, 28(8):1–17, 2006.
[40] T. Gregor, E.F. Wieschaus, A.P McGregor, W. Bialek, and D.W Tank. Stability and nuclear dynamics of the bicoid morphogen gradient. *Cell*, 130:141–152, 2007.
[41] M. N. Gurcan, L. E. Boucheron, A. Can, A. Madabhushi, N. M. Rajpoot, and B. Yener. Histopathological image analysis: A review. *IEEE Reviews in Biomedical Engineering*, 2:147–171, 2009.
[42] R. M. Haralick, K. Shanmugam, and I. Dinstein. Textural features for image classification. *IEEE Transactions on Systems, Man, and Cybernetics*, 3(6):610–621, 1973.
[43] C. L. Luengo Hendriks, S.V.E. Keranen, C. C. Fowlkes, L. Simirenko, G. H. Weber, A. H. DePace, C. Henriquez, D.W. Kaszuba, B. Hamann, M. B Eisen, J. Malik, D. Sudar, M. D. Biggin, and D. W. Knowles. Three-dimensional morphology and gene expression in the drosophila blastoderm at cellular resolution I: Data acquisition pipeline. *Genome Biology*, 7(12):R123, 2006.

[44] R. A. Hess, D. J. Schaeffer, V. P. Eroschenko, and J. E. Keen. Frequency of the stages in the cycle of the seminiferous epithelium in the rat. *Biology of Reproduction*, 43(1):517–524, 1990.
[45] A. K. Jain and F. Farrokhnia. Unsupervised texture segmentation using gabor filters. *Proceedings of IEEE International Conference on Systems, Man and Cybernetics*, pages 14–19, 1990.
[46] J.Canny. A computational approach to edge detection. *IEEE Transactions on Pattern Analysis and Machine Intelligence*, 8(6):679–698, 1986.
[47] V. Jouannet, K. Brackmann, and T Greb. Procambium formation and proliferation: Two sides of the same coin? current opinion in plant biology. *Genome Biology*, 23:54–60, 2015.
[48] M. Kass, A. Witkin, and D. Terzopoulos. Snakes: Active contour models. *International Journal of Computer Vision*, 1(4):321–331, 1988.
[49] J. D. Keeler, D. E. Rumelhart, and W. K. Leow. Integrated segmentation and recognition of hand-printed numerals. *Proceedings of the 1990 Conference on Advances in Neural Information Processing Systems (NIPS 3)*, pages 557–563, 1990.
[50] D. Kierzkowski, M. Lenhard, R. Smith, and C. Kuhlemeier. Interaction between meristem tissue layers controls phyllotaxis. *Developmental Cell*, 26:616–628, 2013.
[51] B. Koeppen and B. Stanton. *Berne and Levy Physiology, 6th edition*. Mosby, an imprint of Elsevier, 2008.
[52] W.W. Ku, R. E. Chapin, R. N. Wine, and B. C. Gladen. Testicular toxicity of boric acid (ba): Relationship of dose to lesion development and recovery in the f344 rat. *Reproductive Toxicology*, 7(4):305–319, 1993.
[53] G. Kylberg, M. Uppström, and I. Sintorn. Virus texture analysis using local binary patterns and radial density profiles. *Progress in Pattern Recognition, Image Analysis, Computer Vision, and Applications. Lecture Notes in Computer Science*, 7042:573–580, 2011.
[54] L. L. Lanning, D. M. Creasy, R. E. Chapin, P. C. Mann, N. J. Barlow, K. S. Regan, and D. G. Goodman. Recommended approaches for the evaluation of testicular and epididymal toxicity. *Toxicologic Pathology*, 30 (4):507–520, 2002.
[55] J. R. Latendresse, A. R. Warbrittion, H. Jonassen, and D. M. Creasy. Fixation of testes and eyes using a modified Davidson's fluid: comparison with Bouin's fluid and conventional Davidson's fluid. *Toxicologic Pathology*, 30:524–533, 2002.
[56] C. P. Leblond and Y. Clermont. Definition of the stages of the cycle of the seminiferous epithelium in the rat. *Journal of the Society of Toxicology*, 55:548–573, 1952.
[57] H.C. Lee and D. R. Cok. Detecting boundaries in a vector field. *IEEE Transactions on Signal Processing*, 39(5):1181–1194, 1991.
[58] C. Li and C. Xu. Distance regularized level set evolution and its application to image segmentation. *IEEE Transactions on Image Processing*, 19(12):3243–3254, 2010.
[59] G. Loy and E. Zelinsky. A fast radial symmetry transform for detecting points of interest. *Pattern Analysis and Machine Intelligence*, 25(8):

959–973, 2003.
[60] R. Malladi, J. A. Sethian, and B. C. Vemuri. Shape modeling with front propagation: A level set approach. *IEEE Transactions on Pattern Analysis and Machine Intelligence*, 17(2):266–277, 1995.
[61] A. Malpani. *How to Have a Baby: Overcoming Infertility*. UBS Publishers Distributors, 2001.
[62] D. Marr and E. Hildreth. Theory of edge detection. *Proceedings of Royal Society of London*, 207:182–217, 1980.
[63] K. Masood and N. M. Rajpoot. Texture based classification of hyperspectral colon biopsy samples using clbp. In *IEEE International Symposium on Biomedical Imaging: From Nano to Macro*, pages 1011–1014, June 2009. doi: 10.1109/ISBI.2009.5193226.
[64] L. M. McClusky, C. de Jager, and M. S. Bornman. Stage-related increase in the proportion of apoptotic germ cells and altered frequencies of stages in the spermatogenic cycle following gestational, lactational, and direct exposure of male rats to p-nonylphenol. *Journal of the Society of Toxicology*, 95:249–256, 2007.
[65] L. M. McClusky, S. Patrick, I. E. Barnhoorn, J. C. van Dyk, C. de Jager, and M. S. Bornman. Immunohistochemical study of nuclear changes associated with male germ cell death and spermiogenesis. *Journal Molelcular Histology*, 40(4):287–299, 2009.
[66] A. L. Mescher. *Junqueira's Basic Histology: Text and Atlas*. McGraw-Hill Medical, 2013.
[67] P. H. T. Nguyen, M. Worring, and R. van den Boomgaard. Watersnakes:energy-driven watershed segmentation. *IEEE Transactions on Pattern Analysis and Machine Intelligence*, 25(3):330–342, 2003.
[68] T. H. Nguyen, S. Sridharan, V. Macias, A. K. Balla, M. N. Do, and G. Popescu. Prostate cancer diagnosis using quantitative phase imaging and machine learning algorithms. *Proceedings of SPIE*, 9336: 933619–933619–10, 2015. doi: 10.1117/12.2080321.
[69] T. Ojala, M. Pietikäinen, and Topi Mäenpää. Gray scale and rotation invariant texture classification with local binary patterns. *IEEE Transactions on Pattern Analysis and Machine Intelligence*, 24(7): 971–987, 2002.
[70] S. Osher and J. Sethian. Fronts propagating with curvature-dependent speed: Algorithms based on hamilton-jacobi formulations. *Journal of Computational Physics*, 79(1):12–49, 1988.
[71] N. Otsu. A threshold selection method from gray-level histograms. *IEEE Transactions on Systems, Man, and Cybernetics*, 9(1):62–66, 1979.
[72] K. Pearson. On lines and planes of closest fit to systems of points in space. *Annals of Eugenics*, 2(6):559–572, 1901.
[73] R.M. Pelletier. Cyclic formation and decay of the blood-testis barrier in the mink (mustela vison), a seasonal breeder. *American Journal of Anatomy*, 175(1):91–117, 1986.
[74] S. Persson, B. Brunström, B.-M. Backlin, H. Kindahl, and U. Magnusson. Wild mink (Neovison vison) as sentinels in environmental monitoring. *Acta Veterinaria Scandinavica*, 54:S9, 2012.

[75] P. Salembier. Morphological multiscale segmentation for image coding. *Signal Processing*, 38(3):359–386, 1994.
[76] S. Sarkar and P. Soundararajan. Supervised learning of large perceptual organization: Graph spectral partitioning and learning automata. *IEEE Transactions on Pattern Analysis and Machine Intelligence*, 22(5): 504–525, 2000.
[77] C. Seiffert, T. M. Khoshgoftaar, J. Van Hulse, and A. Napolitano. Rusboost: A hybrid approach to alleviating class imbalance. *IEEE Transactions on Systems, Man, and Cybernetics: Systems.*, 40(1):185–197, 2009.
[78] O. Sertel, J. Kong, H. Shimada, U. V. Catalyurek, J. H. Saltz, and M. N. Computer-aided prognosis of neuroblastoma on whole-slide images: Classification of stromal development. *Pattern Recognition*, 42(6): 1093–1103, 2009.
[79] J. Shi and J. Malik. Normalized cuts and image segmentation. *IEEE Transactions on Pattern Analysis and Machine Intelligence*, 22(8): 888–905, 2000.
[80] K. Sirinukunwattana, D. R. Snead, and N. M. Rajpoot. A novel texture descriptor for detection of glandular structures in colon histology images. *Proceedings of SPIE*, 9420:94200S–94200S–9, 2015.
[81] T. N. Tan. Rotation invariant texture features and their use in automatic script identification. *IEEE Transactions on Pattern Analysis and Machine Intelligence*, 20(7):751–756, July 1998. doi: 10.1109/34.689305.
[82] X. Tan and B. Triggs. Enhanced local texture feature sets for face recognition under difficult lighting conditions. *IEEE Transactions on Image Processing*, 19(6):1635–1650, 2010.
[83] A. Tashk, M.S. Helfroush, D. H., and M. Akbarzadeh. An automatic mitosis detection method for breast cancer histopathology slide images based on objective and pixel-wise textural features classification. In *5th Conference on Information and Knowledge Technology (IKT)*, pages 406–410, 2013.
[84] D. M. J. Tax, M. Loog, R. P. W. Duin, V. Cheplygina, and W.-J. Lee. Bag dissimilarities for multiple instance learning. *Similarity-Based Pattern Recognition, Lecture Notes in Computer Science*, 7005:222–234, 2011.
[85] L. Vincent and P. Soille. Watersheds in digital spaces: an efficient algorithm based on immersion simulations. *IEEE Transactions on Pattern Analysis and Machine Intelligence*, 13(6):583–598, 1991.
[86] C. Wählby, I. M. Sintorn, F. Erlandsson, G. Borgefors, and E. Bengtsson. Combining intensity, edge and shape information for 2D and 3D segmentation of cell nuclei in tissue sections. *Journal of Microscopy*, 215 (1):67–76, 2004.
[87] Y Wang, R Turner, D Crookes, J Diamond, and P Hamilton. Investigation of methodologies for the segmentation of squamous epithelium from cervical histological virtual slides. *Machine Vision and Image Processing Conference*, pages 83–90, 2007.
[88] A.R. Webb and K. D. Copsey. *Statistical Pattern Recognition, Third Edition*. John Wiley and Sons Ltd, West Sussex, United Kingdoms, 2011.

[89] T. P. Weldon, W. E. Higgins, and D. F. Dunn. Efficient gabor filter design for texture segmentation. *Pattern Recognition*, 29(12):2005–2015, 1996.
[90] Z. Wu and R. Leahy. An optimal graph theoretic approach to data clustering: Theory and its application to image segmentation. *IEEE Transactions on Pattern Analysis and Machine Intelligence*, 11:1101–1113, 1993.
[91] C. Zahn. Graph theoretical methods for detecting and describing gestalt clusters. *IEEE Transactions on Computation*, 20:68–86, 1971.

Acta Universitatis Upsaliensis

Digital Comprehensive Summaries of Uppsala Dissertations from the Faculty of Science and Technology 1262

Editor: The Dean of the Faculty of Science and Technology

A doctoral dissertation from the Faculty of Science and Technology, Uppsala University, is usually a summary of a number of papers. A few copies of the complete dissertation are kept at major Swedish research libraries, while the summary alone is distributed internationally through the series Digital Comprehensive Summaries of Uppsala Dissertations from the Faculty of Science and Technology. (Prior to January, 2005, the series was published under the title "Comprehensive Summaries of Uppsala Dissertations from the Faculty of Science and Technology".)

Distribution: publications.uu.se
urn:nbn:se:uu:diva-252425

ACTA
UNIVERSITATIS
UPSALIENSIS
UPPSALA
2015